Cell Reports

Article

Vangl2 in the Dentate Network Modulates Pattern Separation and Pattern Completion

Graphical Abstract

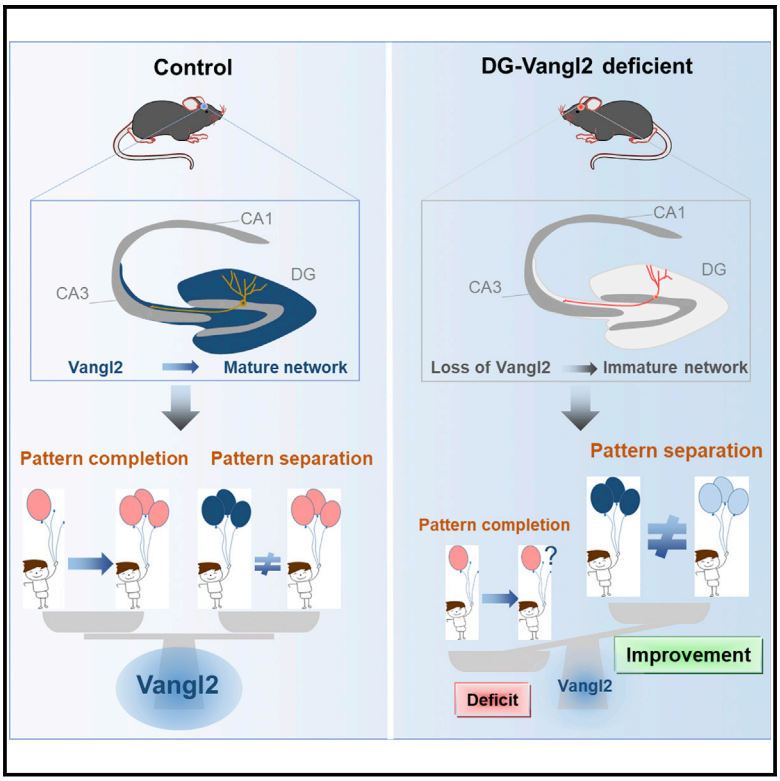

Highlights

- Vangl2-dependent PCP signaling controls granule cell maturation and network integration
- Vangl2 stabilizes GluA1-containing receptors at the surface of dendritic spines
- Granule cells require Vangl2-dependent signaling to elicit LTP
- Vangl2 loss has opposite functional effects on pattern completion/separation processes

Authors

Benjamin J.A. Robert, Maïté M. Moreau, Steve Dos Santos Carvalho, ..., Aline Marighetto, Mireille Montcouquiol, Nathalie Sans

Correspondence

mireille.montcouquiol@inserm.fr (M.M.), nathalie.sans@inserm.fr (N.S.)

In Brief

Robert et al. show that Vangl2 is required for proper granule cell maturation, thus influencing network integration, and that Vangl2 absence in the hippocampus inversely modulates pattern completion and pattern separation. These findings demonstrate inter-independence of the two processes via Vangl2 control of the dentate gyrus network.

Robert et al., 2020, Cell Reports *31*, 107743
June 9, 2020
https://doi.org/10.1016/j.celrep.2020.107743

CellPress

Cell Reports

CellPress
OPEN ACCESS

Article

Vangl2 in the Dentate Network Modulates Pattern Separation and Pattern Completion

Benjamin J.A. Robert,[1,2,9] Maïté M. Moreau,[1,2,9] Steve Dos Santos Carvalho,[1,2,10] Gael Barthet,[3,4,10] Claudia Racca,[5,10] Mehdi Bhouri,[1,2,10] Anne Quiedeville,[1,2] Maurice Garret,[6,7] Bénédicte Atchama,[1,2] Alice Shaam Al Abed,[1,2] Christelle Guette,[1,2] Deborah J. Henderson,[8] Aline Desmedt,[1,2,11] Christophe Mulle,[3,4,11] Aline Marighetto,[1,2] Mireille Montcouquiol,[1,2,12,13,*] and Nathalie Sans[1,2,12,13,14,*]

[1]INSERM, Neurocentre Magendie, U1215, 33000 Bordeaux, France
[2]Université Bordeaux, Neurocentre Magendie, 33000 Bordeaux, France
[3]CNRS, IINS, UMR 5297, 33000 Bordeaux, France
[4]Université Bordeaux, IINS, 33000 Bordeaux, France
[5]Biosciences Institute, Newcastle University, Medical School, Newcastle upon Tyne, NE2 4HH, UK
[6]CNRS, INCIA, 33000 Bordeaux, France
[7]Université Bordeaux, INCIA, 30000 Bordeaux, France
[8]Biosciences Institute, Newcastle University, Centre for Life, Newcastle upon Tyne, NE1 4EP, UK
[9]These authors contributed equally
[10]These authors contributed equally
[11]These authors contributed equally
[12]These authors contributed equally
[13]Senior author
[14]Lead Contact
*Correspondence: mireille.montcouquiol@inserm.fr (M.M.), nathalie.sans@inserm.fr (N.S.)
https://doi.org/10.1016/j.celrep.2020.107743

SUMMARY

The organization of spatial information, including pattern completion and pattern separation processes, relies on the hippocampal circuits, yet the molecular and cellular mechanisms underlying these two processes are elusive. Here, we find that loss of *Vangl2*, a core PCP gene, results in opposite effects on pattern completion and pattern separation processes. Mechanistically, we show that *Vangl2* loss maintains young postmitotic granule cells in an immature state, providing increased cellular input for pattern separation. The genetic ablation of *Vangl2* disrupts granule cell morpho-functional maturation and further prevents CaMKII and GluA1 phosphorylation, disrupting the stabilization of AMPA receptors. As a functional consequence, LTP at lateral perforant path-GC synapses is impaired, leading to defects in pattern completion behavior. In conclusion, we show that Vangl2 exerts a bimodal regulation on young and mature GCs, and its disruption leads to an imbalance in hippocampus-dependent pattern completion and separation processes.

INTRODUCTION

The hippocampus is a key structure for cognition and, notably, learning and memory functions. Remembering spatial representation over time is essential, but it is also crucial to keep memories distinct and resistant to confusion and to retrieve information to rebuild memory representation from partial or altered elements. To achieve these complex tasks, the hippocampus is believed to rely on specific integrative properties of neurons at the single-cell and circuit levels (Rebola et al., 2017; Schmidt-Hieber and Nolan, 2017). Pattern separation, an encoding process allowing memory discrimination, and pattern completion, a recall process allowing memory reconstruction, are two complementary processes thought to rely on the dentate gyrus (DG)/CA3 hippocampal circuitry (Leutgeb et al., 2007; Marr, 1971; McHugh et al., 2007; McNaughton and Morris, 1987). The very sparse firing properties of DG granule cells (GCs), mostly displaying either none or a single place field attached to a single specific context, make GCs good candidates to participate in pattern separation, while CA3 pyramidal cells (PCs) appear critical to perform pattern completion because of the presence of recurrent excitatory collaterals between PCs (Marr, 1971; Mishra et al., 2016; Nakazawa et al., 2002; Rolls, 2013). DG GCs exert a powerful control over the CA3 circuit, not only from direct excitation of CA3 PCs but also through indirect feedforward inhibition (Henze et al., 2002; Torborg et al., 2010). A recent study suggested that GCs participated in both processes depending on their maturation stages, with more excitable young GCs participating in pattern separation, while the less excitable mature GCs are involved in pattern completion processes (Nakashiba et al., 2012). Consistent with this, numerous studies have reported that modulation of proliferation in the adult DG affects pattern separation (Sahay et al., 2011). However, the precise molecular signaling pathway

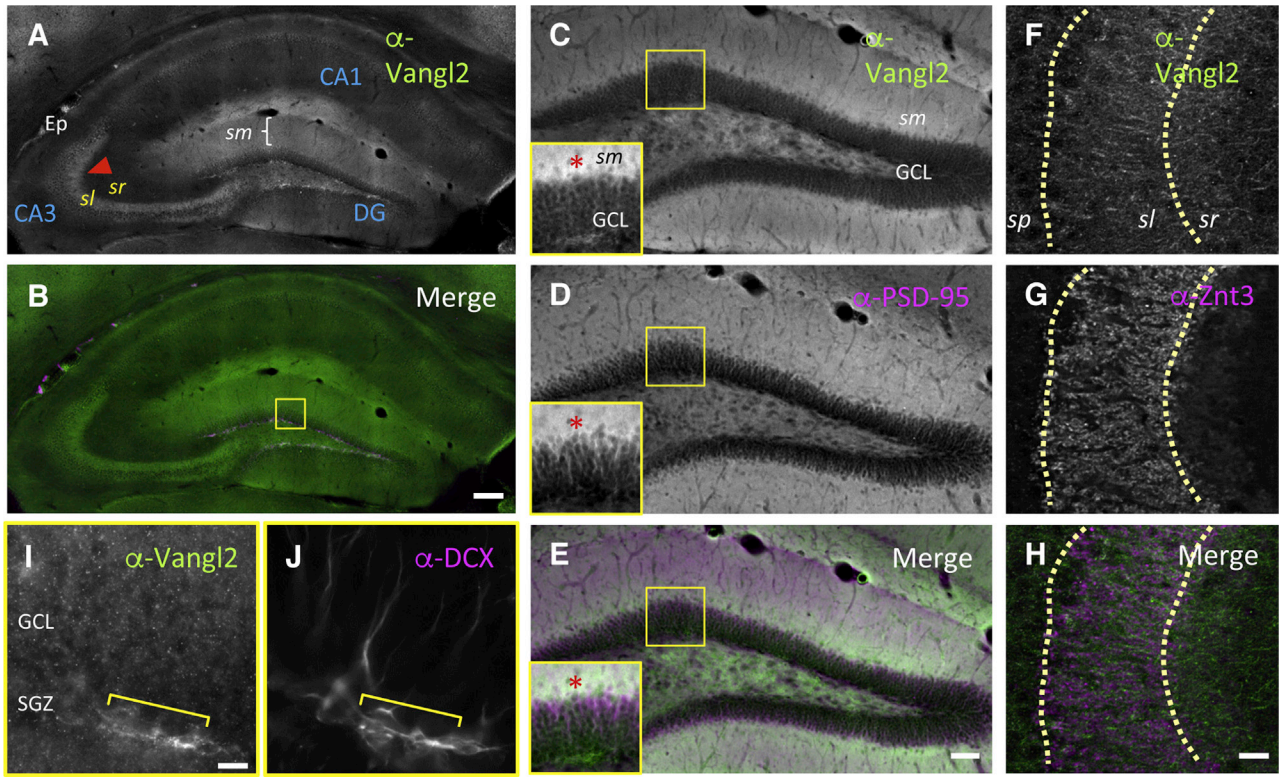

Figure 1. Endogenous Expression of Vangl2 in the Adult Hippocampus

(A and B) Photomicrograph composite stitched from 121 images at 20× magnification of a hippocampal coronal section (10-week-old mouse) immunolabeled with (A) anti-Vangl2 and (B) anti-Vangl2 (green) and anti-DCX (magenta). Vangl2 is notably enriched in the dentate gyrus (DG) molecular layer (*sm*) and in the mossy fibers (red arrowhead) in CA3 stratum lucidum (*sl*).

(C–E) Representative images (10× magnification) of (C) Vangl2 and (D) PSD-95 labeling in DG and (E) overlay of Vangl2 (green) colocalized with PSD-95 (magenta) in GC dendrites in *sm*. Yellow boxes represent the regions where higher magnification (40×) images were taken in DG. Note that Vangl2 is enriched in *sm* (red asterisk), where it colocalizes with PSD-95.

(F–H) Representative images (40× magnifications, with structured illumination) of Vangl2 (F) and Znt3 (G) labeling and (H) overlay of Vangl2 (green) and Znt3 (magenta) in CA3 *sl*.

(I and J) High-magnification images (40×) in the subgranular zone (SGZ) of the image in (B) corresponding to the yellow box. Note that Vangl2 is enriched in SGZ, where it colocalizes with DCX (J) in some hotspots (yellow bracket).

Scale bars, 100 μm (A and B), 50 μm (C–E), and 25 μm (F–J). Ep, ependymal cells; GCL, granule cell layer; *sm*, stratum moleculare; *sp*, stratum pyramidale; *sr*, stratum radiatum. See also Figure S1.

mediating these complex tasks remains unknown. Furthermore, a causal role for a specific pathway among the ones previously associated with these computational processes has yet to be demonstrated.

Here, we show that Van Gogh-like 2 (Vangl2; also known as Vangl planar cell polarity protein 2), a core member of the noncanonical Wnt/planar cell polarity (PCP) signaling pathway in mammals (Montcouquiol et al., 2003, 2006; Montcouquiol and Kelley, 2020; Sans et al., 2016), is enriched in young postmitotic neurons of the neurogenic zone of the adult DG and in all GCs' neurites. We further show that Vangl2 is required for young postmitotic GC maturation and in dendritic arborization and spinogenesis of all GCs. A conditional deletion of *Vangl2* in postmitotic GCs does not alter spatial memory but results in an improved pattern separation combined with impaired pattern completion. Mechanistically we show that the loss of Vangl2-dependent PCP signaling results in decreased phosphorylation levels of CaMKII and GluA1 and an absence of long-term potentiation (LTP) at the lateral perforant path (PP)-GC synapses. We further correlate Vangl2-dependent GluA1 phosphorylation to Vangl2's ability to reduce GluA1-containing AMPAR mobility at synapses. In conclusion, our study uncovers a critical role for PCP signaling in the adult hippocampus function and shows that Vangl2-dependent PCP signaling is necessary for an optimal balance between the "pattern completion" and "pattern separation" processes required for memory function.

RESULTS

Vangl2 Is Enriched in the Adult DG-CA3 Network

Using an in-house-generated antibody (Montcouquiol et al., 2006), we observed a specific enrichment of Vangl2 in DG and CA3 subregions of the hippocampus of 10-week-old mice (Figure 1) that is absent in conditional mutants for Vangl2 (Figure S1). Vangl2 is enriched in DG inner molecular layer (IML) and outer molecular layer (OML), where GC dendrites arborize (Figures 1A–1E),

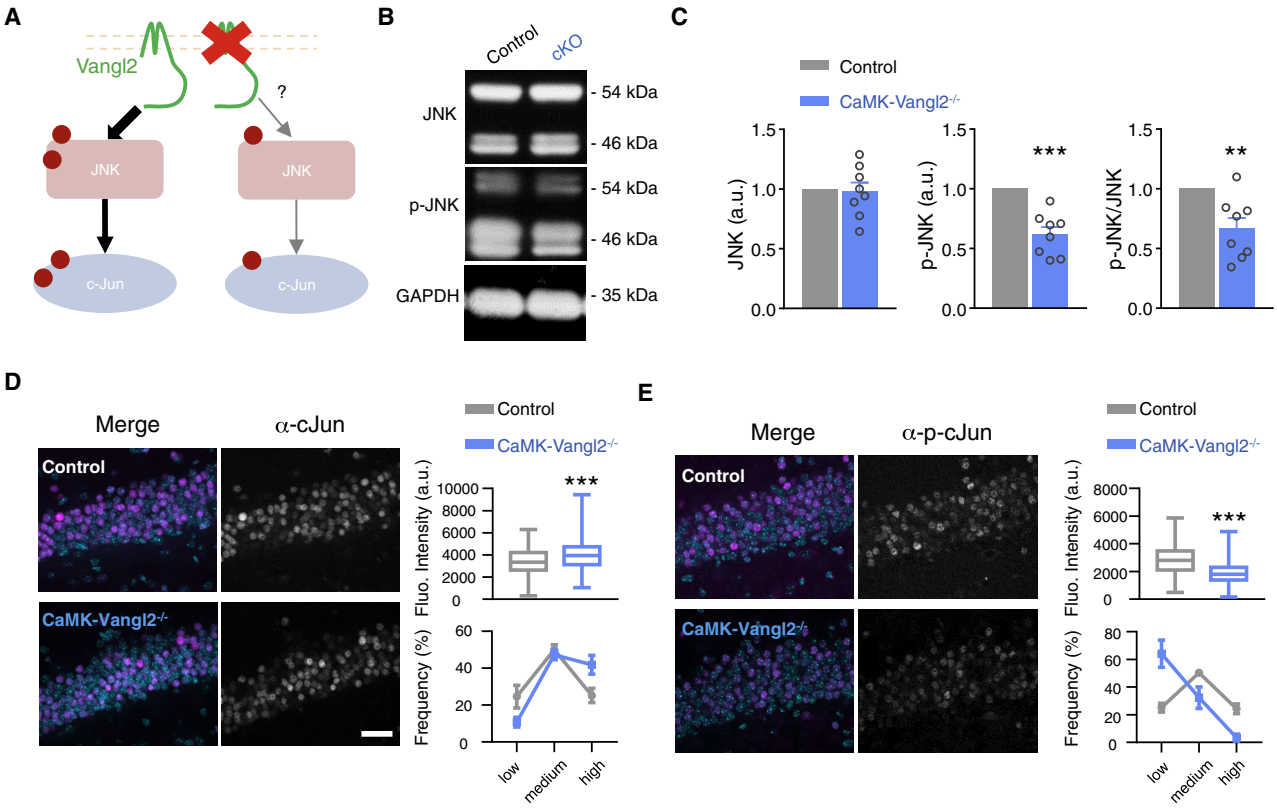

Figure 2. Deletion of Vangl2 Reduces the Activation of the JNK/cJun Pathway

(A) Schematic of Vangl2 protein (green) and the impact of its deletion on SAPK/JNK (pink) and cJun (blue) phosphorylation. Red dots represent phosphorylation sites.

(B and C) Western blots (B) show a decrease in JNK phosphorylation in CaMK-Vangl2$^{-/-}$ mice (C) (n = 6 control mice, n = 8 CaMK-Vangl2$^{-/-}$; $p < 0.001$***, Mann-Whitney test), as confirmed by the ratio JNK phosphorylation to total JNK ($p < 0.01$**, Mann-Whitney test).

(D and E) Immunohistochemistry of hippocampal sections: (D) increased fluorescence intensity of cJun signal in DG GCs of CaMK-Vangl2$^{-/-}$ mice compared with control (n = 4 control mice, n = 4 CaMK-Vangl2$^{-/-}$; $p < 0.001$***, Mann-Whitney test); (E) decreased fluorescence intensity of p-cJun signal in DG GCs of CaMK-Vangl2$^{-/-}$ mice compared with control ($p < 0.001$***, Mann-Whitney test). Merge images are pseudocolored: DAPI (cyan) and cJun or p-cJun (magenta). Values are mean ± SEM. Scale bar: 40 μm.

**$p < 0.01$ and ***$p < 0.001$. See also Table S1.

as well as in CA3 stratum lucidum, where mossy fibers (Mfs) make synaptic contacts on the proximal apical dendrites of CA3 PCs (Figures 1A, 1B, and 1F–1H). Vangl2 is also present in DG neurogenic subgranular zone (SGZ), where it colocalizes in some hotspots with doublecortin (DCX)-positive cells, a marker of young postmitotic GCs (Figures 1B, 1I, and 1J). We detected weaker Vangl2 labeling in the DG GC layer, which also contains the somata of more mature GCs (Figures 1A–1C). These data are consistent with the enrichment of Vangl2 in the soma (and likely neurites) of young postmitotic GCs at the time of their maturation and in mature GC dendrites and Mfs, which connect GCs to mossy cells, GABAergic neurons, and CA3 PCs. Thus, the localization pattern of Vangl2 in dendrites and axons is consistent with a role in regulating GC morphogenesis and DG-CA3 network connectivity pre- and postsynaptically.

Loss of Vangl2 Impairs PCP Signaling

To investigate the role of *Vangl2* in network function and restrict its deletion to postnatal neurons, we created transgenic conditional knockout (cKO) *Vangl2$^{f/f}$::CaMKII-cre* mice, henceforth called CaMK-Vangl2$^{-/-}$ (see STAR Methods; Figure S1A). We confirmed that the Cre-Lox recombination occurred in the vast majority of hippocampal PCs and GCs using an Ai6 reporter or PCR amplification (Figures S1B and S1C). As a result, Vangl2 protein was virtually absent in the hippocampus of 10-week-old mice (Figures S1D and S1E). CaMK-Vangl2$^{-/-}$ mice did not exhibit gross abnormalities in brain size or morphology (data not shown), including in the hippocampus (Figure S1F).

Unlike the canonical Wnt pathway, there is no common and consensual transcriptional readout of the activation of PCP signaling, as it is mainly known to modulate cytoskeleton reorganization. However, in some systems, the non-canonical Wnt/PCP signaling has been shown to activate JNK signaling (Boutros et al., 1998; Puvirajesinghe et al., 2016; Shafer et al., 2011; Vivancos et al., 2009; Weber et al., 2000; Yamanaka et al., 2002). We observed a significant reduction in phosphorylated JNK (p-JNK) protein levels in DG of CaMK-Vangl2$^{-/-}$ mice compared with controls, supporting the activation of JNK

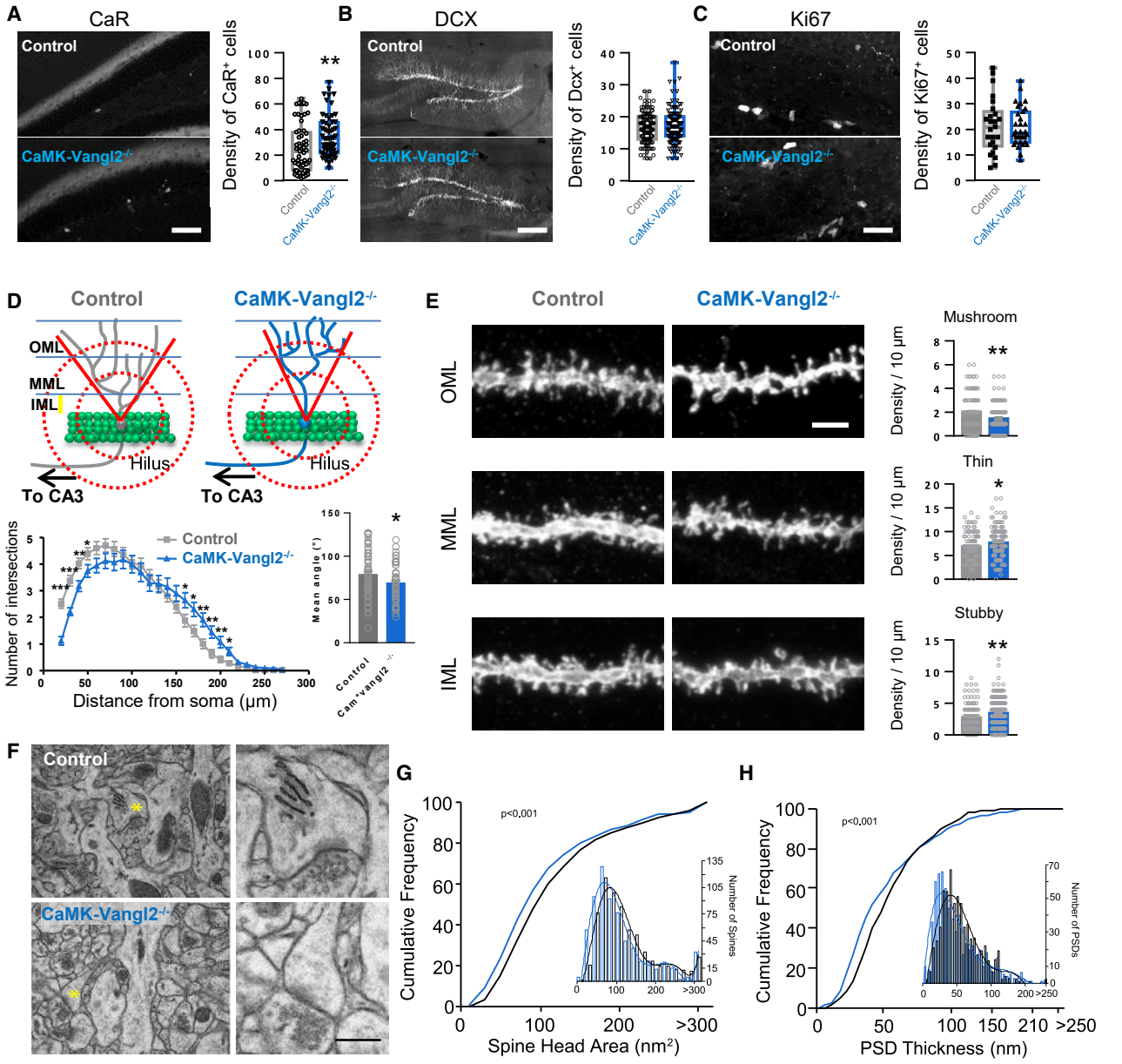

Figure 3. CaMK-Vangl2$^{-/-}$ Mice Show Immature Features in the Dentate Gyrus

(A–C) Immunohistochemistry of hippocampal sections: (A) increased number of CaR-positive cells per lamina in multiple DG sections of CaMK-Vangl2$^{-/-}$ mice compared with control (n = 4 mice for both groups; p = 0.0026**, unpaired t test); (B) no differences in the density of DCX-positive cells (n = 3 mice for both groups; p = 0.4071, unpaired t test) or (C) Ki67 positive cells, suggesting a delay in the transient phase of immaturity without affecting cell proliferation (n = 3 mice for both groups; p = 0.5614, unpaired t test).

(D) Schematic of Golgi stained GC tracing (top). Sholl analysis quantification (bottom left) and global angle of the dendritic arborization (bottom right). In CaMK-Vangl2$^{-/-}$ GCs present reduced proximal arborization, increased branching in the distal part (n = 5 mice for both groups; unpaired t test; table statistics show detail related to each point), and reduced angle of the dendritic tree (n = 5 mice for both groups, p = 0.0323*).

(E) Ten micrometer dendrite segments of GCs in outer membrane layer (OML), middle membrane layer (MML), and inner membrane layer (IML) regions of the molecular layer (left). Mice were injected with a lentivirus driving the expression of a membrane YFP to quantify and classify dendritic spines (right). There is a significant decrease in the number of mushroom spines in OML in CaMK-Vangl2$^{-/-}$ mice compared with controls (n = 128 dendrites for control and n = 127 for CaMK-Vangl2$^{-/-}$; p = 0.0053**, Mann-Whitney U test) and an increase in thin or stubby spines in MML and IML, respectively (n = 132 dendrites for control and n = 158 for CaMK-Vangl2$^{-/-}$, p = 0.0290*, unpaired t test; n = 127 dendrites for control and n = 205 for CaMK-Vangl2$^{-/-}$, p = 0.0018**, Mann-Whitney U test).

(F) Representative low-magnification electron micrographs of DG OML of control and CaMK-Vangl2$^{-/-}$ mice (top and bottom left) and higher magnifications (top and bottom right) of a spinous synapse, marked by an asterisk in the respective low-magnification panels.

(G) Shifted distribution of spine head area. Control, 127.09 ± 3.14 nm (n = 3 mice for both groups); CaMK-Vangl2$^{-/-}$, 117.99 ± 3.56 nm (n = 3 mice for both groups) (p < 0.001***, Mann-Whitney rank-sum test).

(legend continued on next page)

signaling by Vangl2 in our model (Figures 2A–2C). Further analysis shows a significant increase in the average fluorescence intensity of GCs expressing cJun and a concomitant decrease in cells expressing p-cJun in the absence of Vangl2 (Figures 2D and 2E). The number of cells containing higher amounts of cJun was increased in CaMK-Vangl2$^{-/-}$ mice, to the detriment of low-containing ones (Figure 2D), while the proportion of cells containing lower amounts of p-cJun was increased in CaMK-Vangl2$^{-/-}$ mice to the detriment of high-containing ones (Figure 2E). The ratio of p-cJun over total cJun confirmed a significant decrease in CaMK-Vangl2$^{-/-}$ mice compared with control (59% phosphorylation ratio in CaMK-Vangl2$^{-/-}$ mice compared with control normalized at 100%, n = 4 for each condition, p = 0.0286). This result together with the decrease of p-JNK demonstrate that Vangl2 deletion in GCs leads to a partial inhibition of the JNK signaling pathway. Altogether, these results suggest that Vangl2 contributes to the activation of the JNK signaling pathway in the adult mammalian DG.

Vangl2-Dependent Signaling Regulates GC Maturation

Because Vangl2 is enriched in the SGZ, we studied whether the absence of *Vangl2* could affect DG maturation, using calretinin (CaR) as a marker for immature GCs (Kempermann et al., 2004). As expected, CaR labeling was sparsely found in the cells of the proliferative zone of DG control mice (Figure 3A). This number increased statistically in CaMK-Vangl2$^{-/-}$ mice (Figure 3A). However, there was no difference in the number of DCX-positive cells or Ki67-positive (a cell proliferation marker) cells (Figures 3B and 3C), suggesting that the overall number of young postmitotic (i.e., newly produced and immature cells) GCs was not affected; the latter finding is consistent with the restriction of CaMKIIα expression to postmitotic neurons (Arruda-Carvalho et al., 2014; Casanova et al., 2001). Because immature GCs lack functional perisomatic GABAergic inhibition (Toni and Schinder, 2015), we used CaR antibodies to visualize immature neurons in DG, together with the presynaptic vesicular GABA transporter (VGAT) and the postsynaptic cell adhesion protein Neuroligin-2 (NL2) to label inhibitory synapses. There was no difference between the two genotypes in the number of VGAT and NL2 puncta on the cell periphery of CaR-positive cells, suggesting that the additional immature GCs in CaMK-Vangl2$^{-/-}$ mice received the same number of inhibitory inputs as controls (Figure S2). Altogether, our results suggest that the absence of Vangl2 delays GC maturation, leading to supernumerary immature GCs in the adult DG, independently of proliferation.

Loss of Vangl2 Results in GC Structural Deficits

The structural complexity of dendrites, dendritic spine morphology, and synapse number can be considered as markers of GC functional integrity, and they critically depend on cytoskeleton, the main target of PCP signaling (Zhao et al., 2006). The tracing of GC arborization in CaMK-Vangl2$^{-/-}$ mice showed a reduction in the complexity of the proximal part of the dendritic tree, which mostly receives input from the axons of associative/commissural mossy cells. The distal part of the dendritic tree, which mostly receives input from the axons of layer II entorhinal cortex neurons via the lateral and medial PP, was more ramified in CaMK-Vangl2$^{-/-}$ GCs than controls (Figure 3D). Furthermore, the angle formed by the two most extreme branches of the dendritic tree was reduced in CaMK-Vangl2$^{-/-}$ GCs (Figure 3D). YFP viral labeling of GC neurites showed a significant decrease in the number of mushroom spines in the DG OML in CaMK-Vangl2$^{-/-}$ mice compared with controls (Figure 3E, OML). This decrease was concomitant with an increase in thin and stubby spines in the middle molecular layer (MML) and the IML, respectively (Figure 3E). Electron microscopy analysis (Figure 3F) confirmed a shifted cumulative probability curve toward smaller spine head area (Figure 3G) and postsynaptic density (PSD) thickness (Figure 3H). Specifically, spines from CaMK-Vangl2$^{-/-}$ GCs were more likely to be smaller and have thinner PSDs than those of controls. These results indicate that postmitotic *Vangl2* deletion alters (1) arborization and (2) spinogenesis, which could affect both connectivity and integration of GCs in the network.

Early Postnatal Deletion of Vangl2 Improves Pattern Separation Function

Postnatal deletion of *Vangl2* in CaMK-Vangl2$^{-/-}$ mice has no impact on working memory in the Y-maze, locomotor activity, exploration, or anxiety (Figure S3). Challenged through a radial maze task (Clelland et al., 2009) (Figures S4A and S4B), CaMK-Vangl2$^{-/-}$ mice performed better than controls, regardless of pattern separation difficulty level (Figures S4C–S4E). Because the improvement was not dependent on task difficulty, we next submitted the mice to a contextual fear discrimination task as a second test of pattern separation (see STAR Methods; Figure 4A) (Desmedt et al., 2003; Nakashiba et al., 2012). Importantly, to render the discrimination challenging and prevent any simple cue-based discrimination, the two contexts differed only in their distal background cues. During block 1 (days 2–4), CaMK-Vangl2$^{-/-}$ mice discriminated better the aversive context from the neutral one than the controls, as CaMK-Vangl2$^{-/-}$ mice displayed higher levels of freezing than controls in the conditioning context only (Figures 4B and 4D). During block 2 (days 5–8), there was no difference between controls and CaMK-Vangl2$^{-/-}$ mice, and both groups displayed higher levels of freezing in conditioning context than in neutral context (Figures 4C and 4E). These results show that CaMK-Vangl2$^{-/-}$ mice were able to discriminate between two similar contexts faster than control mice, indicating an improvement of pattern separation process in the absence of Vangl2.

Early Postnatal Deletion of Vangl2 Impairs Pattern Completion without Altering Spatial Learning

CaMK-Vangl2$^{-/-}$ mice were next submitted to a pattern completion behavioral test in the Morris water maze (Figure 4F). We did

(H) Shifted distribution of PSD thickness (right) toward smaller values in the DG OML of CaMK-Vangl2$^{-/-}$ compared with control (black). Control, 57.92 ± 1.19 nm (n = 3 mice for both groups); CaMK-Vangl2$^{-/-}$, 54.92 ± 1.44 nm (n = 3 mice for both groups) (p < 0.001***, Mann-Whitney rank-sum test).

Values are mean ± SEM. Scale bars, 50 μm (A), 8 μm (B), 625 nm (C), 2 μm (E), 100 μm (F, top and bottom left), and 340 nm (F, top and bottom right). *p < 0.05 and **p < 0.01. See also Figure S2 and Table S1.

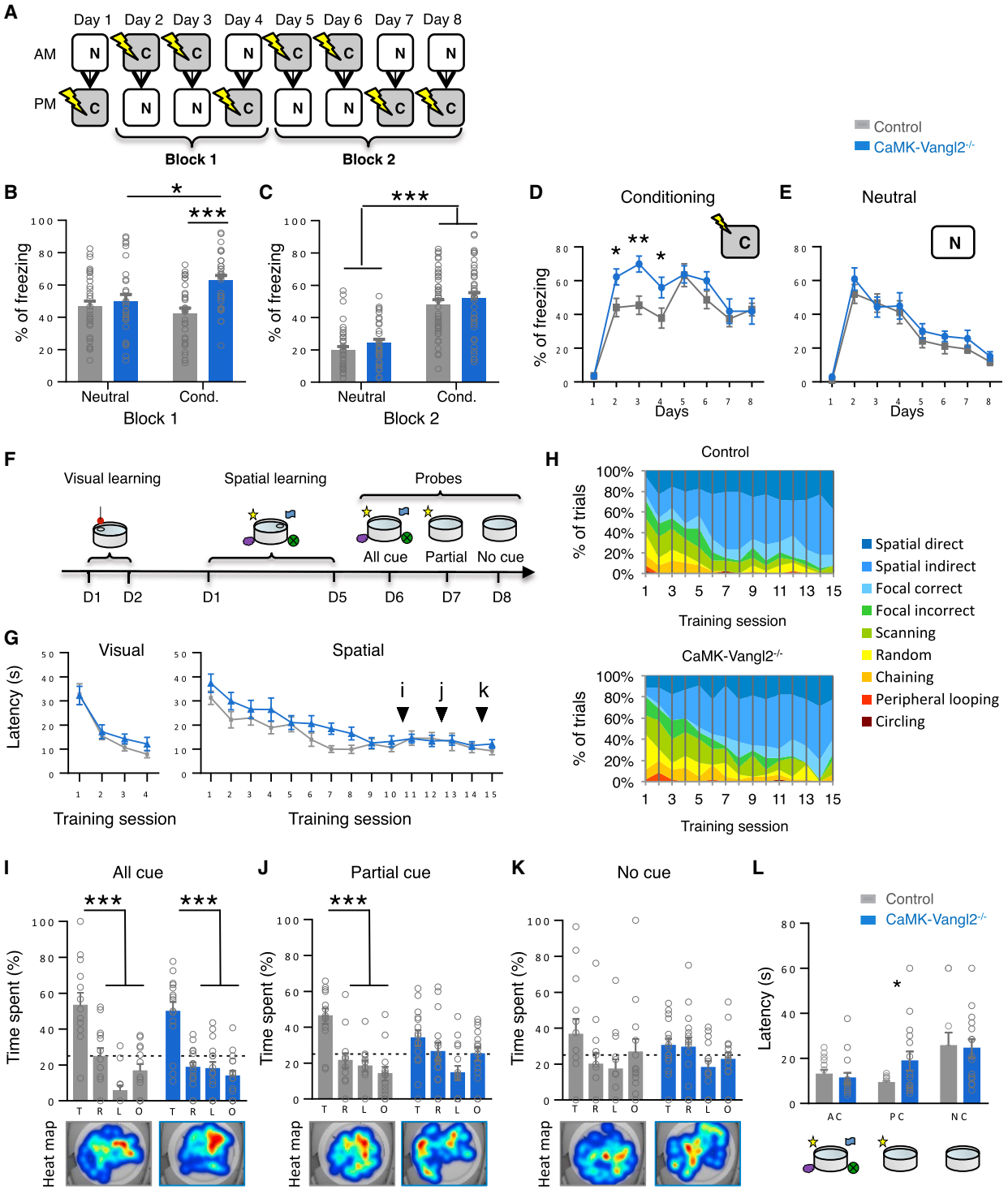

Figure 4. CaMK-Vangl2$^{-/-}$ Mice Perform Better in Contextual Fear Discrimination Tasks Requiring "Pattern Separation" and Exhibit Deficits in Spatial Pattern Completion Task

(A) Design of the contextual fear discrimination experiment. Mice visit both neutral context (N) and conditioning context (C) every day in a pseudo-random fashion, during 8 days.

(B and C) Mean of freezing of both groups in neutral or conditioning context (B) during the first block and (C) during the second block of training. CaMK-Vangl2$^{-/-}$ exhibited a higher level of freezing in conditioning context compared with neutral context and compared with controls during the first block (n = 11 control mice, n = 10 CaMK-Vangl2$^{-/-}$; two-way ANOVA, context × genotype interaction: $F_{[1, 122]} = 5.862$, p = 0.0169*; genotype: $F_{[1, 122]} = 11.59$, p = 0.0009***; n = 11 control

(legend continued on next page)

not observe differences between CaMK-Vangl2$^{-/-}$ and control mice in the latency to reach the cued platform during the visual learning (Figure 4G, visual), hence their willingness to swim to escape the water and their visual acuity were not affected by *Vangl2* deletion. In the spatial learning, CaMK-Vangl2$^{-/-}$ mice reached the platform more slowly than did control mice in the first part of the training, but they eventually reached the same level of performance as controls at the end of training (Figure 4G, spatial). We showed that the delay observed for the CaMK-Vangl2$^{-/-}$ group was due to mutant mice's using preferentially a research strategy (Ruediger et al., 2012) that was more systematic than the spatial strategy used by controls (Figure 4H). In the probe test, both groups spent approximately 50% of the time on the phantom platform (PPF) and less than 25% in other quadrants, demonstrating that the absence of Vangl2 does not impair hippocampus-dependent spatial memory (Figure 4I). To test for pattern completion, we removed some of the spatial cues and re-evaluated the time spent in each quadrant. When most cues were removed, CaMK-Vangl2$^{-/-}$ mice spent equal time in each quadrant (~25%), while the controls continued to show preference for the target (~45%) (Figure 4J). Both groups were lost in the no-cue condition, confirming the need for some spatial cues to locate the platform (Figure 4K). We also observed a significantly higher latency to reach the platform in CaMK-Vangl2$^{-/-}$ mice than in controls in the partial-cue probe test (Figure 4L). To summarize, CaMK-Vangl2$^{-/-}$ mice can form new spatial memories but are impaired when they need to retrieve these memories from partial cues, highlighting a defect in pattern completion.

Postnatal Deletion of Vangl2 Abolishes the Ability of GCs to Elicit LTP

We evaluated the impact of the loss of *Vangl2* on intrinsic membrane and synaptic properties of GCs in 10-month-old CaMK-Vangl2$^{-/-}$ and control mice acute hippocampal slices (Figure 5A). First, we performed whole-cell voltage-clamp experiments to analyze basal synaptic transmission and plasticity at the lateral PP (LPP) onto the DG. Excitatory postsynaptic currents (EPSCs) were evoked at different stimulation intensities to assess the input/output (I/O) relationship at LPP-DG GC synapses (Figure 5B). The I/O relationship in CaMK-Vangl2$^{-/-}$ mice was not different from that of controls. The amplitude and frequency of AMPAR-mediated miniature EPSCs (mEPSCs; Figure 5C) were unaltered in mutants, demonstrating that the number of functional synapses and the levels of synaptic AMPAR were unaffected by Vangl2 loss. Paired-pulse ratios at multiple interstimulus intervals were also unchanged in mutants (Figure 5D). To assay synaptic NMDAR content, we evoked dual-component EPSCs and measured AMPAR/NMDAR ratios, which exhibited no difference in CaMK-Vangl2$^{-/-}$ mice (Figure 5E). Finally, we investigated LTP at LPP-DG GC synapses by recording field excitatory postsynaptic potential (fEPSP) before and after a high-frequency stimulation (HFS) protocol (Figure 5F). The HFS protocol induced LTP in DG in most slices in controls (success rate close to 90%), but scarcely in slices from CaMK-Vangl2$^{-/-}$ mice (success rate 17%) (Figure 5F). Altogether, these data indicate that whereas *Vangl2* deletion does not affect basal synaptic transmission and short-term plasticity, it abolishes LTP at LPP-DG GC synapses.

We found a significant reduction in the phosphorylation level of GluA1-containing receptors at residues S831 and S845 while GluA1 levels remain unchanged in the DG of CaMK-Vangl2$^{-/-}$ mice (Figure 5G). We also found a reduction in the phosphorylation state of CaMKII in mutant mice (Figure 5H). GluA1-containing AMPAR dynamics and/or phosphorylated forms can affect LTP, and CaMKII is known for its role in GluA1-containing receptor phosphorylation at S831 and in the consequent increase of channel conductance. Specifically, GluA1 phosphorylation at

mice, n = 10 CaMK-Vangl2$^{-/-}$; Bonferroni's multiple-comparisons test: control: neutral versus conditioning, $t_{[122]} = 0.8792$, $p > 0.05$; CaMK-Vangl2$^{-/-}$ neutral versus conditioning, $t_{[122]} = 2.507$, $p < 0.05$*; conditioning: control versus CaMK-Vangl2$^{-/-}$, $t_{[122]} = 4.12$, $p < 0.001$***). During the second block, both groups exhibited a higher level of freezing in the conditioning context (n = 11 control mice, n = 10 CaMK-Vangl2$^{-/-}$ mice; two-way ANOVA, context × genotype interaction: $F_{[1, 164]} = 0.00879$, $p = 0.9254$; genotype: $F_{[1, 164]} = 11.59$, $p = 0.1278$; context: $F_{[1, 164]} = 107.7$, $p < 0.0001$***).

(D and E) Percentage of freezing during 8 days, (D) in conditioning context and (E) in neutral context. CaMK-Vangl2$^{-/-}$ mice exhibited a higher level of freezing from day 2 to 4 compared with controls only in conditioning context (n = 11 control mice, n = 10 CaMK-Vangl2$^{-/-}$ mice; two-way ANOVA repeated measures [RM], genotype [days 1–4]: $F_{[1, 19]} = 10.52$, $p < 0.0043$**; Bonferroni's multiple-comparisons test: control versus CaMK-vangl2$^{-/-}$, day 2: $t_{[76]} = 2.671$, $p < 0.05$*; day 3: $t_{[76]} = 2.614$, $p < 0.01$**; day 4: $t_{[76]} = 3.614$, $p < 0.05$*).

(F) Design of the Morris water maze task. Mice are trained during 5 days to find the platform using spatial cues around the maze. Spatial memory is tested in probe test with all cues. "Pattern completion" is tested when cues are partially removed.

(G) A trend toward a delay in learning can be observed for CaMK-Vangl2$^{-/-}$ (n = 13 mice for control [gray], n = 15 CaMK-Vangl2$^{-/-}$ mice [blue]; two-way RM ANOVA, training session × genotype interaction: $F_{[14, 364]} = 0.8294$, $p = 0.6370$; genotype: $F_{[1, 26]} = 3.869$, $p = 0.0599$#; training session: $F_{[14, 364]} = 14.43$, $p < 0.0001$***). Black arrows represent probe tests.

(H) Strategy used by mice during spatial learning. CaMK-Vangl2$^{-/-}$ mice use spatial strategy (blue) later than control mice, corresponding to the delay observed in latency.

(I–K) Bars show the percentage of time spent in each PPF. (I) With all cues, both groups spent longer in the target PPF compared with other quadrants (n = 13 control mice, n = 15 CaMK-Vangl2$^{-/-}$ mice; two-way ANOVA, PPF × genotype interaction: $F_{[3, 104]} = 1.756$, $p = 0.1601$; genotype: $F_{[1, 104]} < 0.0001$, $p > 0.05$; PFF: $F_{[3, 104]} = 34.04$, $p < 0.0001$***; Bonferroni's multiple-comparisons: control and cKO target versus others, $p < 0.001$***). (J) With partial cues, only controls spent longer in target compared with all others (two-way ANOVA, PPF × genotype interaction: $F_{[3, 104]} = 3.011$, $p = 0.0335$*; genotype: $F_{[1, 104]} < 0.0001$, $p > 0.05$; PFF: $F_{[3, 104]} = 12.97$, $p < 0.0001$***; Bonferroni's multiple-comparisons: control target versus others, $p < 0.001$***; cKO target versus left: $p < 0.01$**, cKO target versus others: $p > 0.05$). (K) Without any cue, both groups were lost in the water maze (two-way ANOVA, PPF × genotype interaction: $F_{[3, 104]} = 0.7509$, $p > 0.05$; genotype: $F_{[1, 104]} < 0.0001$***, $p > 0.05$; PFF: $F_{[3, 104]} = 2.593$, $p > 0.05$).

(L) Control and CaMK-Vangl2$^{-/-}$ mice reached the phantom platform (PPF) with similar delay with all-cue and no-cue conditions but not with partial cues (n = 13 control mice, n = 15 CaMK-Vangl2$^{-/-}$ mice; unpaired t test with Welch's correction: $t_{[14, 91]} = 2.259$, $p = 0.0393$*). Dotted lines represent the chance. T, target; R, right; L, left; O, opposite; AC, all cues; PC, partial cues; NC, no cues.

Values are mean ± SEM. #$p < 0.10$, *$p < 0.05$, **$p < 0.01$, and ***$p < 0.001$. See also Figures S3 and S4 and Table S1.

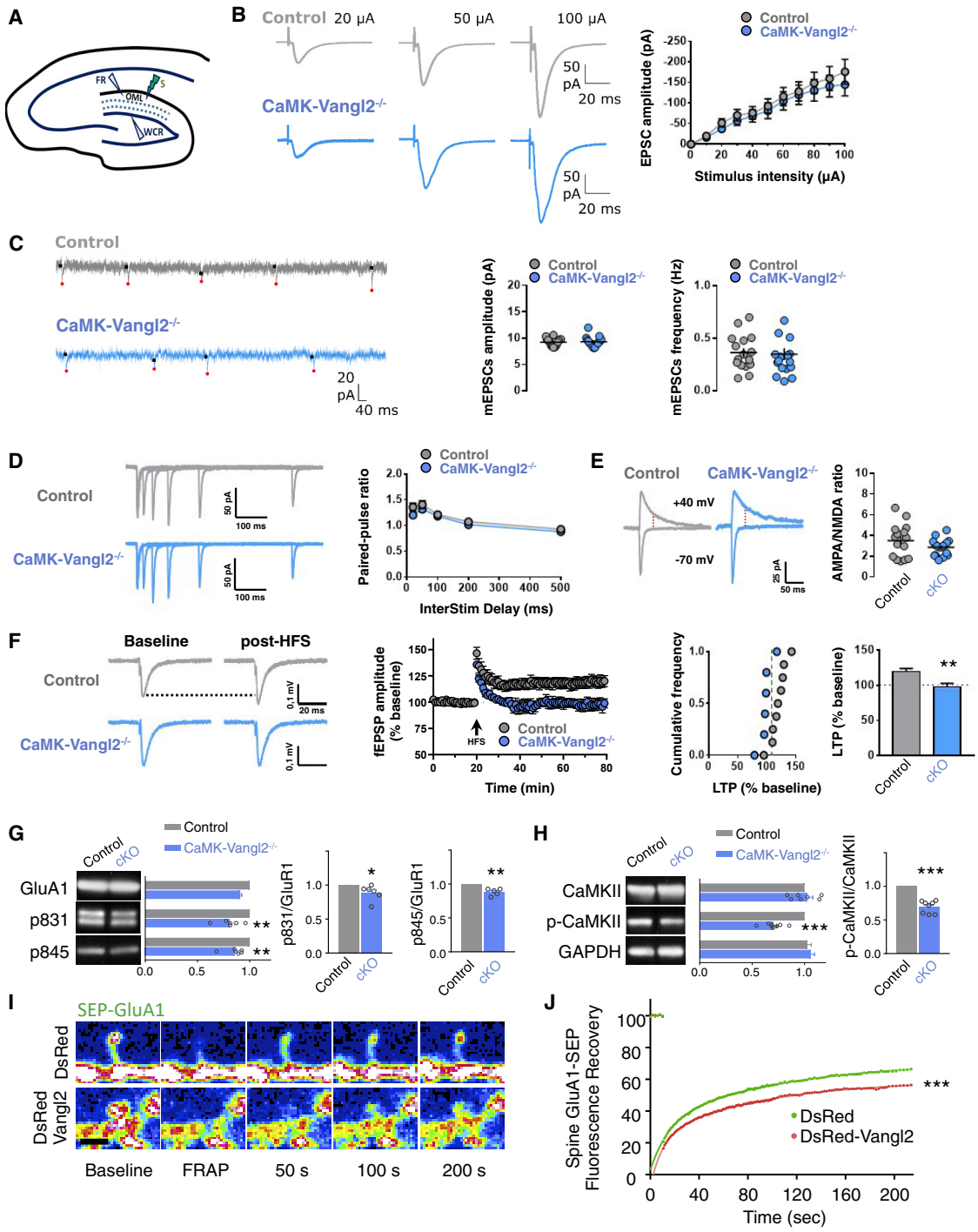

Figure 5. Vangl2 Contributes to LTP Maintenance through the Regulation of AMPAR Stabilization at the Spine Surface

(A) Schematic of a hippocampal slice showing recording and stimulating electrodes positioning in DG outer molecular layer (OML). FR, field recording; WCR, whole-cell recording; S, stimulation.

(B) Representatives traces (left) and summary graph (right) showing the input/output relationship for control (gray dots; n = 12 neurons) and CaMK-Vangl2$^{-/-}$ mice (blue dots; n = 12 neurons). The stimulation intensity was increased from 10 to 100 μA. Traces at 20, 50, and 100 μA are shown. No significant difference was observed (two-way ANOVA).

(C) Representatives traces (left) and summary plots (right) of mean miniatures EPSCs (mEPSCs) amplitude (left; p = 0.90, Mann-Whitney test) and mESPC frequency (right; p = 0.51, Mann-Whitney test) for control (gray dots; n = 16 neurons) and CaMK-Vangl2$^{-/-}$ mice (blue dots; n = 17 neurons). Detected mEPSCs are depicted by black squares (onset) and red points (peak). The amplitude and the frequency are unchanged.

(legend continued on next page)

S845 is known to promote the insertion of these receptors at the cell surface of spines (Diering and Huganir, 2018). Our functional results suggest that Vangl2 participates in the regulation of GluA1 phosphorylation via the activation of CaMKII signaling and ultimately in the induction of LTP via an increase of channel conductance. Hence, we measured the mobility of GluA1 molecules (SEP-GluA1) at the surface of neurons using FRAP, along with Vangl2 coupled to DsRed or DsRed alone as a control (Figure 5I). Under control conditions, the SEP-GluA1 signal recovered up to 71% of pre-bleach levels at the end of our protocol, while the concomitant coexpression of DsRed-Vangl2 led to a significant reduction of signal recovery (Figures 5I and 5J). As FRAP experiments do not allow to assess whether the return of SEP-GluA1 signal is related to the lateral mobility or to exo- or endocytosis of these receptors, we conclude that Vangl2 plays a role in the stabilization and/or lateral mobility SEP-GluA1 at the synapse membrane. Together with the immunoblot analysis, showing a reduction in CaMKII and GluA1 phosphorylation, and the impairment of synaptic plasticity at LPP-DG GC synapses, these results strongly suggest that Vangl2 stabilizes GluA1-containing receptors at the surface of spines and that its loss affects the maintenance of LTP in GCs.

Spatial Completion Is Rescued When Vangl2 Is Re-introduced in the DG of CaMK-Vangl2$^{-/-}$ Mice

To confirm the role of Vangl2 in the GCs of the DG during pattern separation processes, we attempted a rescue of CaMK-Vangl2$^{-/-}$ mice by re-expressing *Vangl2* under the control of a CaMKIIα promoter using AAV2/9-CaMKII(0.4)-mCherry-2A-Vangl2 or AAV2/9-CaMKII(0.4)-mCherry as a control virus in the DG of control and CaMK-Vangl2$^{-/-}$ mice (Figures 6A and 6B). Although no significant difference among the groups was observed for the visual task in the Morris water maze, the CaMK-Vangl2$^{-/-}$ mice injected with the mCherry-Vangl2 virus (referred as CaMK-Vangl2^{Resc}) reached the platform significantly faster along the training sessions than the CaMK-Vangl2$^{-/-}$ that were injected with the control virus (Figure 6C). In the all-cue probe test, all the groups were able to locate the platform (Figure 6D). In the partial-cue condition, CaMK-Vangl2$^{-/-}$ mice were less accurate in locating the platform than in the all-cue condition, as seen previously (Figure 4J), and they were also less accurate than the control and CaMK-Vangl2^{Resc} mice (Figure 6E). Performance deficits were observed in the control mice injected with *Vangl2*/mCherry, suggesting that a fine balance in Vangl2 levels is necessary for its optimal function in the hippocampus, a result consistent with prior studies reporting that the core PCP pathway is highly gene dose dependent (Torban et al., 2008). Finally, all the groups performed poorly in the no-cue probe test (Figure 6F). In conclusion, re-expression of *Vangl2* in DG GCs of adult CaMKII-Vangl2$^{-/-}$ mice was sufficient to rescue the deficit in the spatial pattern completion task.

Late and DG-Specific Deletion of Vangl2 Impairs Pattern Completion and Improved Pattern Separation Processes

The CaMK-Vangl2$^{-/-}$ mutant we used so far presents deletion of *Vangl2* in other brain regions that takes effect during the first week after birth and reaches a high level after 3 weeks (Casanova et al., 2001; Hilal et al., 2017). To confirm the specific role of *Vangl2* via the GCs, we next used a viral strategy. We injected the DG of 5-week-old *Vangl2*$^{f/f}$ mice with LV-C1ql2-ChIEFTomato-2A-Cre (or LV-C1ql2-ChIEFTomato in a parallel cohort) using a C1ql2 minimal promoter specific to GCs (Barthet et al., 2018) (see STAR Methods; Figure 7A; Figure S5). Five weeks after infection, both the DG-Vangl2^{Control} and DG-Vangl2^{CRE} cKO (henceforth called DG-Vangl2^{cKO}) mice displayed strong expression of ChIEF-Tomato (Ch-Tomato) in the DG along the rostrocaudal axis (Figure 7B; Figure S5B). Approximately 60% of neurons were immunoreactive to an anti-CRE antibody (Figure S5C), and we observed an 80% decrease in Vangl2 protein levels compared with controls (Figure S5D). We confirmed a significant reduction of JNK activation in DG-Vangl2^{cKO} mice compared with DG-Vangl2^{Control} (Figures S6A and S6B), as observed previously (Figure 2). In the contextual fear discrimination protocol (Figure 4A), DG-Vangl2^{cKO} mice exhibited a higher level of freezing than control mice in the conditioning context during block 1 (days 2–4) (Figures 7C and 7E), while similar levels of freezing were observed in the neutral context (Figure 7C). During

(D) Representative traces (left) and summary graph (right) of paired-pulse ratios at different stimulus intervals for control (gray dots; n = 14 neurons) and CaMK-Vangl2$^{-/-}$ mice (blue dots; n = 13 neurons). No significant difference was observed (two-way ANOVA).
(E) Representative traces of AMPA and NMDA EPSCs (left) and summary plots of mean AMPA/NMDA ratios (right) for control (gray dots; n = 15 neurons) and CaMK-Vangl2$^{-/-}$ mice (blue dots; n = 17 neurons). NMDAR EPSCs were measured at 40 ms (red vertical dashed line) after the onset of the dual-component EPSC at +40 mV. p = 0.15, t test.
(F) Representatives traces (left), summary graph (middle), and cumulative frequency plots (right) showing that LTP is abolished in CaMK-Vangl2$^{-/-}$ mice 50–60 min after HFS. Cumulative frequency plot of the magnitude of fEPSP change for all individual experiments. The LTP of fEPSP is decreased from 120% to 96% (n = 9 control slices control and n = 6 CaMK-Vangl2$^{-/-}$ slices; p = 0.008**, unpaired t test).
(G) Decrease of GluA1 phosphorylation for both P831 (106 kDa) and P845 (106 kDa) residues (n = 6 control mice and n = 8 CaMK-Vangl2$^{-/-}$; p < 0.001**, Mann-Whitney test) and of GluA1 (106 kDa) phosphorylation (both residues) over total GluA1 (p < 0.05* and p < 0.001**, Mann-Whitney test) after Vangl2 deletion in DG of CaMK-Vangl2$^{-/-}$ adult mice compared with control.
(H) Decrease of CaMKII phosphorylation (50 kDa; n = 6 control mice and n = 8 CaMK-Vangl2$^{-/-}$; p < 0.001***, Mann-Whitney test) and of CaMKII phosphorylation over total CaMKII (50 kDa; p < 0.01**, Mann-Whitney test) in DG of CaMK-Vangl2$^{-/-}$ adult mice compared with controls. GADPH molecular weight ~35 kDa.
(I) Control condition (DsRed, top panel) and Vangl2-overexpression condition (DsRed-Vangl2, lower panel) images of GluA1-SEP in spines of dissociated neurons. Scale bar: 3.5 μm.
(J) GluA1-SEP fluorescence on spines of neurons overexpressing DsRed-Vangl2 (red dotted line) recovered less after photobleaching than corresponding controls (DsRed neurons: fluorescence plateau = 71%, n = 130 spines from 26 neurons versus DsRed-Vangl2 neurons: fluorescence plateau = 59%, n = 198 spines from 28 neurons) (data fitted with a non-linear two-phase associated fit: p < 0.001***).
Values are mean ± SEM. *p < 0.05, **p < 0.01, and ***p < 0.001. See also Table S1.

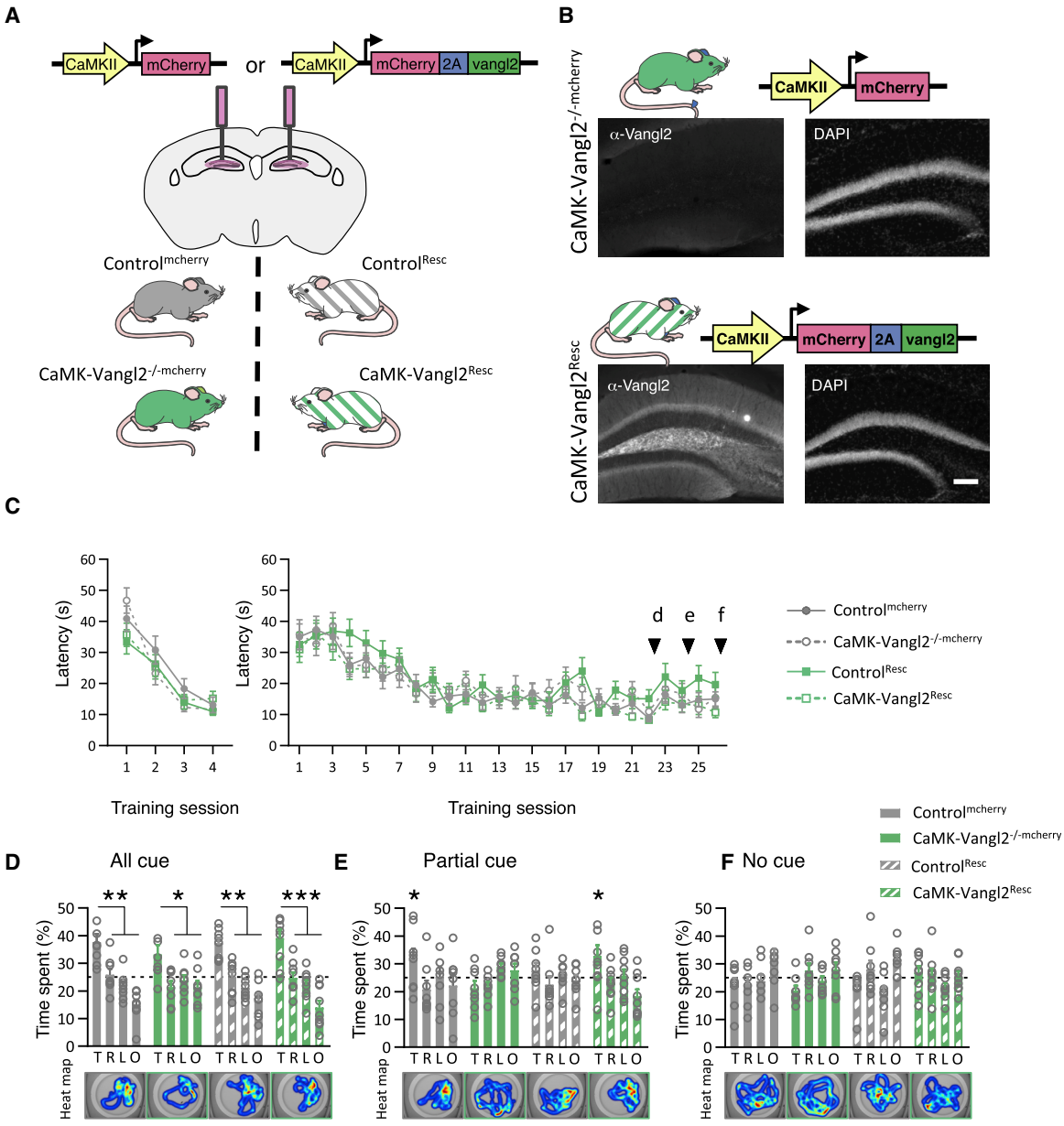

Figure 6. CaMK-Vangl2$^{-/-}$ Mice with Vangl2 Re-expressed in DG Granule Cell Exhibit a Rescue in Spatial Pattern Completion

(A) Schematic of the transgenes carried by the AAVs injected bilaterally in DG of controls (gray or gray stripes) or CaMK-Vangl2$^{-/-}$ mice (green or green stripes) and the corresponding mice. The mice injected with the virus containing the *vangl2* transgene are labeled "rescue" (Resc).

(B) Immunohistochemistry with an anti-Vangl2 antibody of hippocampal sections of CaMKII-Vangl2$^{-/-}$ injected with control virus or rescue virus containing the *vangl2* transgene, illustrating the effective overexpression of Vangl2 in the DG of CaMKII-Vangl2^{Resc} mouse.

(C) CaMK-Vangl2$^{-/-}$ mice (green, n = 8), control littermates (gray, n = 8) injected with control virus and CaMK-Vangl2$^{-/-}$ rescued mice (green stripes, n = 9), control rescued (gray stripes, n = 8) were trained in visual learning and spatial learning test. A significant difference is observed between CaMK-Vangl2$^{-/-}$ and CaMK-Vangl2^{Resc} during spatial learning (two-way RM ANOVA: genotype: $F_{[3, 95]} = 4.198$, p = 0.0078**; Tukey's multiple-comparisons test: CaMK-Vangl2$^{-/-}$ versus CaMK-Vangl2^{Resc}, p = 0.0066**). Black arrows represent probe tests.

(D–F) Bars show the percentage of time spent in each quadrant. (D) With all cues, all groups spent longer in the target PPF compared with other quadrants (two-way ANOVA: quadrant × genotype interaction: $F_{[9, 116]} = 1.408$, p = 0.1927; genotype: $F_{(3, 116)} < 0.0001$, ***p > 0.9999; quadrant: $F_{[3, 116]} = 54.99$, p < 0.0001***; Tukey's multiple-comparisons test: all groups, target versus others, *p < 0.05, **p < 0.01, and ***p < 0.001). (E) With partial cues, only controls and CaMK-Vangl2^{Resc} spent longer in target quadrant compared with CaMK-Vangl2$^{-/-}$ and control rescued (two-way ANOVA: quadrant × genotype interaction: $F_{[9, 116]} = 2.047$, p = 0.0400*; genotype: $F_{[3, 116]} < 0.0001$, p > 0.9999; quadrant: $F_{[3, 116]} = 4.374$, p = 0.0059**; Tukey's multiple-comparisons test: control versus CaMK-Vangl2$^{-/-}$, p = 0.0499*; CaMK-Vangl2$^{-/-}$ versus CaMK-Vangl2^{Resc}, p = 0.0164*). (F) Without any cue, both groups were lost in the water maze (two-way ANOVA:

(legend continued on next page)

block 2 (days 5–8), while DG-Vangl2^{cKO} mutants still displayed higher level of freezing than DG-Vangl2^{Control} mice in the conditioning context, both groups discriminated the two contexts (Figure 7D). Overall, DG-Vangl2^{cKO} displayed higher levels of freezing to the aversive context than to the neutral context across the 8 days of training, whereas DG-Vangl2^{Control} mice showed a similar level of freezing in both contexts, except during the second block (Figures 7C–7F).

In the Morris water maze protocol (Figure 4F), both groups performed similarly in the visual and spatial learning tasks (Figure 7G) and showed similar performance for the all cue probe test (Figure 7H). However, when we removed part of the spatial cues, DG-Vangl2^{cKO} mice were impaired in their ability to find the platform location (Figure 7I). Finally, both groups were lost in the no-cue condition (Figure 7J). In conclusion, the late and DG-specific deletion of *Vangl2* leads to improvements in pattern separation and deficits in pattern completion.

DISCUSSION

In this study, we investigated the role of Vangl2 in hippocampus-dependent computational processes. Our experiments provide evidence for a key role of Vangl2 in morpho-functional plasticity of GCs in the DG and in the integration of critical level of computation for memory processes. We demonstrate that both early and late conditional deletions of *Vangl2* affect computational functions that are thought to rely on the DG-CA3 network, namely, "pattern completion" and "pattern separation," while sparing other abilities to learn hippocampus-dependent tasks. Importantly, the absence of Vangl2 in adult DG was sufficient to affect pattern separation and completion in an opposite way, suggesting that Vangl2 participates in maintaining a functional balance between these two processes in the brain. Mechanistically, our results show that by controlling postmitotic GC maturation and AMPAR mobility, Vangl2 regulates DG network connectivity, synaptic plasticity, and specific cognitive functions in the adult brain.

The Core PCP Protein Vangl2 Regulates Hippocampal GC Maturation and Connectivity

We identified the core PCP protein Vangl2 as an important and specific regulator of hippocampal maturation and function. We showed that although *Vangl2* transcription occurs in the brain during early stages of postnatal development, it becomes prominent in the DG and CA3 regions of the hippocampus. Because the main target of core PCP signaling is the modulation of the cytoskeleton (Babayeva et al., 2011; Dos-Santos Carvalho et al., 2020), it was expected that Vangl2 would regulate the branching of dendritic trees and spine density in the brain. Deletion of *Vangl2* in GCs also led to decreased levels of p-JNK and p-cJun in GCs. JNK activation is believed to be a downstream effector of Vangl2 in specific cellular contexts (Boutros et al., 1998; Davey and Moens, 2017; Puvirajesinghe et al., 2016; Shafer et al., 2011; Vivancos et al., 2009; Weber et al., 2000; Yamanaka et al., 2002), but JNKs are also important in CNS morphogenesis, as illustrated by the embryonic lethality of JNK1/JNK2 double-mutant mice that present severe neural tube defects (NTDs), a phenotype found in many PCP gene mutants, including *Vangl2* (Sabapathy et al., 1999). However, although JNKs are responsible for cJun phosphorylation, more than 100 proteins have now been reported as JNK substrates, and their activation can affect cellular survival but also cytoskeletal or cell-cell adhesion proteins (Zeke et al., 2016).

Recent studies have shown that *in vitro* downregulation of *Vangl2* using short hairpin RNA (shRNA), or the spontaneous *Looptail* mutant, led to a global decrease in dendritic arborization and/or spine number in dissociated hippocampal or cortical neurons (Hagiwara et al., 2014; Nagaoka et al., 2014; Okerlund et al., 2016). Others reported a similar reduction in dendritic tree complexity in newborn GCs using similar molecular tools for other core PCP genes such as Fz3 or Celsr2 and Celsr3 (but not Celsr1) in adult DG *in vivo* (Schafer et al., 2015). In contrast with these results, Zou and colleagues reported an increased spine density in the hippocampal CA1 region of postnatal day (P) 14 mice, in a cKO of *Vangl2* with a different spatiotemporal deletion of *Vangl2* initiated at P7 (Thakar et al., 2017). Our present results paint a complex picture of the consequences of the deletion of *Vangl2 in vivo*, with differences in the various molecular layers of the DG in terms of both dendritic arborization complexity and spine density. As a result, the connectivity is most probably affected with complex functional consequences. This complex phenotype may result from the dual distribution of Vangl2 protein during the maturation period of GCs, with an enrichment of Vangl2 in the somata of immature postmitotic GCs and a massive redistribution to the neurites of mature GCs. This expression profile seems to correlate with the dual functional impact we observed when *Vangl2* is deleted, namely, delayed maturation of immature GCs and disruption of normal neuritogenesis in more mature GCs. Indeed, the increase of CaR-positive cells in the SGZ of the DG in the absence of *Vangl2* shows that Vangl2 is required to properly terminate GCs maturation. The molecular basis of this is unknown, but PCP regulation of neural growth could be a conserved mechanism of PCP signaling, as Vangl2 inhibition in planarian or during *Xenopus* development and tail regeneration also resulted in increased neural growth (Beane et al., 2012).

A Role for Vangl2-Dependent Signaling in LTP Maintenance and Stabilization of AMPAR at Synapses

In vertebrates, CaMKII is an effector of the Wnt-Ca^{2+} and PCP pathways (Kohn and Moon, 2005), and our data confirm that loss of Vangl2 affected CaMKII phosphorylation in mouse hippocampus. Our results suggest that a reduction of Vangl2-dependent PCP signaling in the DG interferes with the activation of CaMKII, thus reducing GluA1 phosphorylation (S831 and S845) and affecting LTP at LPP-DG GC synapses. It has been shown

quadrant × genotype interaction: $F_{[9, 116]} = 1.586$, $p = 0.1331$; genotype: $F_{[3, 116]} < 0.0001$, $p > 0.9999$; quadrant: $F_{[3, 116]} = 6.966$, $p = 0.0002$***). Dotted lines represent the chance. T, target; R, right; L, left; O, opposite.
Values are mean ± SEM. *$p < 0.05$, **$p < 0.01$, and ***$p < 0.001$. See also Table S1.

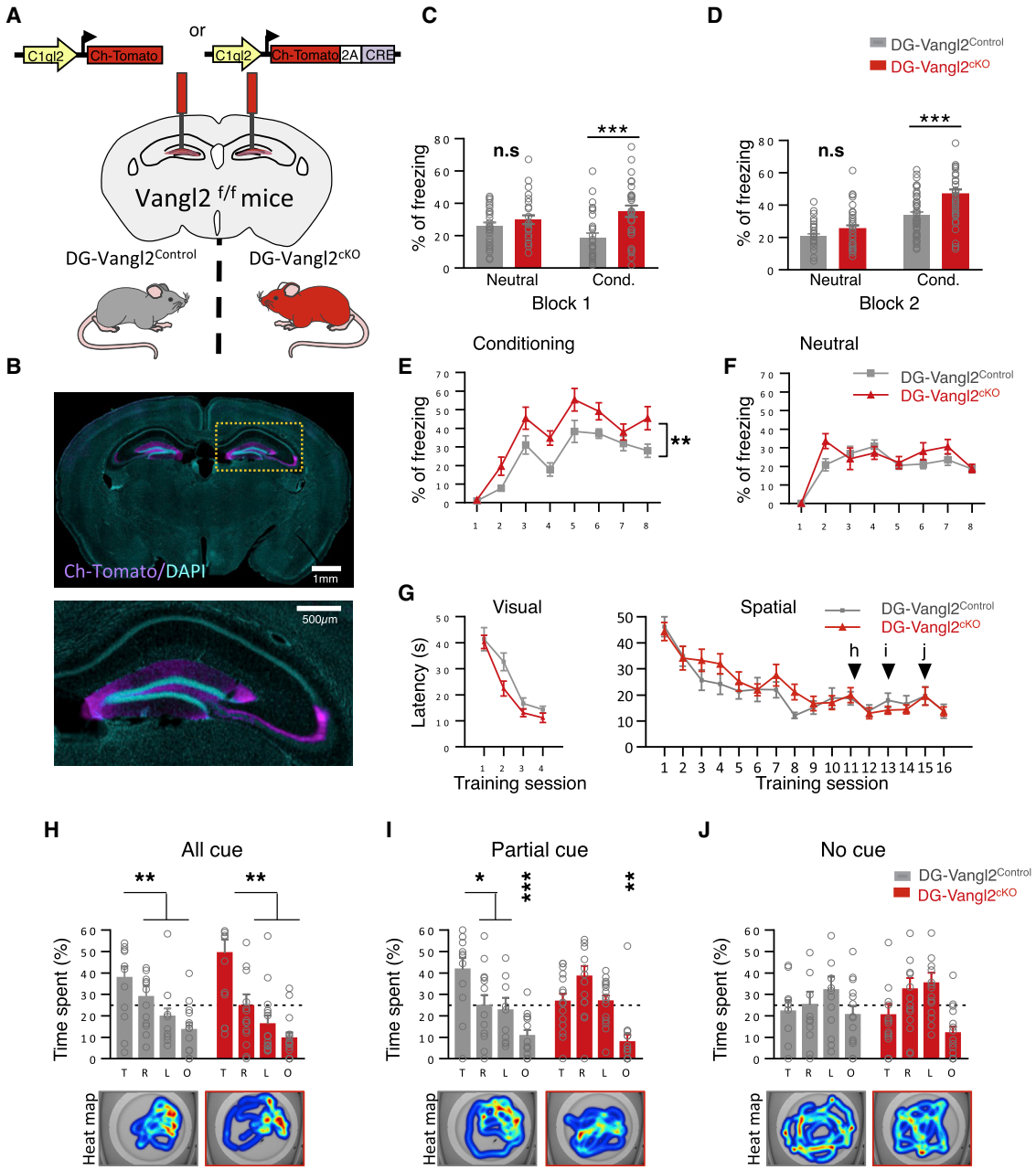

Figure 7. DG-Vangl2^{cKO} Mice Exhibit Deficits in Spatial Pattern Completion and Exhibit Better Performance in Contextual Fear Discrimination Task Requiring Pattern Separation

(A) Schematic of the transgene which co-expresses ChIEF fused to the fluorescent protein tomato (Ch-Tomato) without and with CRE recombinase carried by the lentivirus injected bilaterally in the DG. The promoter C1ql2 restricts expression to DG.

(B) Representative image of a coronal section of a vangl2$^{f/f}$ mouse brain injected with the lentivirus coding for ChIEFtomato-2A-CRE (Ch-Tomato in magenta, DAPI in blue).

(C and D) Mean of freezing of both groups in neutral or conditioning context. (C) During the first block (two-way ANOVA: context × genotype interaction: $F_{[1, 110]} = 5.028$, $p = 0.0269$*; genotype: $F_{[1, 110]} = 12.79$, $p = 0.0005$***; Bonferroni's multiple-comparisons test: conditioning, DG-Vangl2^{control} versus DG-Vangl2^{cKO}, $p < 0.001$***). (D) During the second block of training (two-way ANOVA: context × genotype: $F_{[1, 148]} = 3.971$, $p = 0.0481$*; genotype: $F_{[1, 148]} = 16.19$, $p < 0.0001$***; Bonferroni's multiple-comparisons test: conditioning, DG-Vangl2^{control} versus DG-Vangl2^{cKO}, $t_{[148]} = 4.254$, $p < 0.001$***).

(E and F) Percentage of freezing during the 8 days, (E) in conditioning context (two-way ANOVA RM: genotype [days 1–8]: $F_{[1, 18]} = 13.95$, $p = 0.0015$**) and (F) in neutral context (two-way ANOVA RM: genotype [days 1–8]: $F_{[1, 18]} = 1.442$, $p > 0.05$). Deletion of Vangl2 leads to an improvement of pattern separation in a fear conditioning task.

(G) DG-Vangl2^{cKO} mice exhibited normal visual and spatial learning during the training in water maze. Black arrows represent probe tests.

(legend continued on next page)

that CaMKII signaling is key to the induction of maximal LTP, as it promotes GluA1 targeting to the PSD (Sun et al., 2005). Moreover, GluA1-containing AMPAR phosphorylated at S831 residue is enriched at PSDs and acts to target or stabilize GluA1 at the cell surface, while phosphorylation at S845 promotes GluA1-containing AMPAR trafficking at the surface (Diering and Huganir, 2018; Esteban et al., 2003). As a consequence of these decreases in phosphorylation, GluA1-containing AMPAR localization at the membrane of spines would be affected. Here, we show that in the presence of Vangl2, spines have a larger fraction of immobile GluA1-containing AMPAR. We propose that the suppression of *Vangl2* leads to a decrease of CaMKII activation and a reduction in phosphorylation of GluA1-containing AMPAR. Consequently, the targeting of GluA1-containing AMPARs at synapses is decreased, abolishing the ability to express LTP at LPP-DG GC synapses while the basal synaptic transmission remains unchanged.

These results contrast with a recent study using a different *Vangl2* conditional mutant in which the authors reported an increase in mEPSC frequencies that they correlated to an increased number of spines in the CA1 region (Thakar et al., 2017). The very different and somewhat problematic nature of the SLICK-A-Cre-line used in that study makes comparison with our own results complicated for two reasons: first, because there is no excision of *Vangl2* in the CA3 in this transgenic mouse and, second, because the stage of recording (2- to 3-week-old mice) and the region recorded (CA1) are different (Heimer-McGinn and Young, 2011). The increase in mEPSCs and synaptic density in the CA1 region observed by Thakar et al. (2017) could result from transient and early phase in the adaptation of the network to Vangl2 decrease occurring during or shortly before recordings and from the inherent immaturity of the circuitry. It has been shown that the inhibition of CA1 synaptic pruning, which peaks around P21 (Jawaid et al., 2018), leads to a transient increase in synapse number and increased mEPSC frequencies and amplitudes in 2- and 3-week-old mice (Paolicelli et al., 2011). One could imagine that Vangl2 participates in this CA1 pruning and that, in its absence, synapse density is not correctly reduced. Further electrophysiology in the SLICK-A transgenic could provide further proof that this is or not a transient phenomenon.

Specific Consequences of Vangl2 Absence in Hippocampal Cognitive Functions

Classic computational theories of the mnemonic functions of the hippocampus suggest that CA3 mediates pattern completion, DG mediates pattern separation, and both processes compete to provide an adaptive response on the basis of environmental demand (Newman and Hasselmo, 2014). A recent study further suggested that while young adult-born GCs play a key role in pattern separation, mature GCs are required for rapid pattern completion (Nakashiba et al., 2012). Our results from *Vangl2* mutants fit this theory and suggest that Vangl2 participates in a balance between pattern separation and pattern completion, notably by modulating GC maturation and GluA1 mobility. Moreover, loss of Vangl2 causes what resembles a reverse alteration of what is seen in aging, which we correlated to an increase of immature GCs. The idea of a putative balance between the two memory processes fits a small but growing literature suggesting that spatial pattern completion becomes prevalent in humans as a result of normal aging and at the expense of pattern separation. This balance may occur because of age-related changes in subregions of the hippocampus, including a decrease in DG neurogenesis (Stark et al., 2010; Yassa et al., 2011; Wilson et al., 2006; Holden and Gilbert, 2012). Our study demonstrates that by simply shutting down Vangl2-dependent signaling in postnatal GCs, thus not altering proliferation, it is possible to maintain a pool in an immature state and/or reshape their neurite arborization to modulate with opposite consequences pattern completion and separation processes. Importantly, *Vangl2* deletion does not affect all hippocampus-dependent processes. The various *Vangl2* cKO mice we generated do not exhibit "classical" spatial memory deficits. Moreover, we did not observe a disruption in Mf-CA3 synaptic transmission with the loss of Vangl2. Our findings are opposite to those of two recent studies on another core PCP gene that reported deficits in the Morris water maze, Barnes maze, and contextual fear conditioning tests in conditional mutant mice for *Celsr3* (Feng et al., 2012; Thakar et al., 2017). Both studies, however, had limitations. In the former study, the Morris water maze was performed with very young mice (P17–P21), while in the latter study, an inducible SLICK-A-CreER line was used to delete *Celsr3*. As mentioned, this line is somewhat problematic in terms of spatiotemporal specificity. More globally, caution should be exercised in generalizing the role of PCP signaling in the developing and adult brain, and comparisons between the core PCP genes should be carefully drawn with respect to the evolution of the function of these genes. One of the best examples is *flamingo*, an atypically large cadherin and the furthest upstream of the core PCP proteins, that fulfils a "classical" core PCP function in the epithelia and also controls axon guidance in *Drosophila* neurons (Lee et al., 2003). In mammals, however, these two functions appear to have been segregated, with *Celsr1* serving a bona fide core PCP function in inner ear epithelia while *Celsr3* has little impact on epithelial PCP but is important for axon guidance (Feng et al., 2012). This multiplicity might also explain the

(H–J) Bars show the percentage of time spent in each quadrant. (H) With all cues, both groups spent much longer in the target PPF compared with other quadrants (two-way ANOVA: quadrant × genotype interaction: $F_{[3,\ 108]} = 1.454$, $p = 0.2313$; quadrant: $F_{[3,\ 108]} = 18.63$, $p < 0.0001$***; Tukey's multiple-comparison test: quadrant effect, target versus others, $p < 0.01$). (I) With partial cues, only DG-Vangl2^{control} mice spent longer in target compared with all others, while DG-Vangl2^{cKO} spent equal time in all PPF (two-way ANOVA: quadrant × genotype interaction: $F_{[3,\ 108]} = 3.962$, $p = 0.0101$*; Tukey's multiple-comparison test: DG-Vangl2^{cKO}, target versus opposite, $p < 0.01$**, target versus others, $p > 0.05$; control, target versus opposite, $p < 0.0001$***, target versus others, $p < 0.05$*). (J) Without any cue, both groups were lost in the water maze (two-way ANOVA; quadrant × genotype interaction: $F_{[3,\ 108]} = 0.8994$, $p = 0.4441$; quadrant: $F_{[3,\ 108]} = 4.666$, $p = 0.0042$**; Tukey's multiple-comparison test: target versus others, $p > 0.05$). Dotted lines represent the 25% chance to spend time in a PPF randomly. T, target; R, right; L, left; O, opposite.

Values are mean ± SEM. *$p < 0.05$, **$p < 0.01$, and ***$p < 0.001$. See also Figures S5 and S6 and Table S1.

lack of expected phenotypes in shRNA experiments when only one of the members is downregulated (Schafer et al., 2015).

Vangl2 in Pathological Contexts

Vangl1 and *Vangl2* mutations have been reported in patients with variability in terms of phenotypic consequences, including NTDs and frequent hydrocephalus combined with Chiari II (Arnold-Chiari) malformation (Torban et al., 2008). The presence of hydrocephalus prevents accurate evaluation of specific cognitive disruption in these patients, but our mutant models show a role for *Vangl2* in cognitive alteration. Emerging evidence suggests that maturation of GCs is a key factor in mental health. An "immature DG" has been associated with several neuropsychiatric pathologies, such as schizophrenia and bipolar disorders, that could lead to pattern separation deficits (Hagihara et al., 2013; Tamminga et al., 2012). However, in these studies, the number of immature cells in the DG is dramatically increased, much more so than that in our mutants, while the number of mature neurons is highly decreased with the DG transmitting non-orthogonalized information to CA3, further resulting in an overgeneralization (Altar et al., 2005; Ohira et al., 2013; Walton et al., 2012; Yamasaki et al., 2008). In conclusion, our data support the notion that *Vangl2* participates in the development and support of hippocampus-related functions involved in maintaining the balance between pattern separation and pattern completion.

STAR★METHODS

Detailed methods are provided in the online version of this paper and include the following:

- KEY RESOURCES TABLE
- RESOURCE AVAILABILITY
  - Lead Contact
  - Materials Availability
  - Data and Code Availability
- EXPERIMENTAL MODEL AND SUBJECT DETAILS
  - Mice
  - Plasmids, virus and stereotaxic injection
- METHOD DETAILS
  - Immunohistochemistry
  - Tissue extracts, SDS-PAGE, WB analysis
  - Golgi impregnation method
  - Timm's staining
  - Quantification of dendritic spines
  - Neuronal cell culture
  - FRAP and analysis
  - Electron Microscopy Analysis
  - Electrophysiological recordings
  - Behavioral testing
- QUANTIFICATION AND STATISTICAL ANALYSIS

SUPPLEMENTAL INFORMATION

Supplemental Information can be found online at https://doi.org/10.1016/j.celrep.2020.107743.

ACKNOWLEDGMENTS

We thank Prof. Dr. G. Schütz and colleagues for the CaMKII-Cre mice (DKFZ, Germany); C. Medina, C. Blanchard, M. Decroo, R. Peyroutou, J. Rumi-Masante, E. Navarro, A. Ferreira, and L. Brayda-Bruno for technical assistance; and M. Carta and S. Fievre for critical comments on the manuscript. We thank the personnel of the Animal Facility of the Neurocentre Magendie for the mouse care (notably M. Jacquet); the personnel of the genotyping facility (notably D. Gonzales and her team); the personnel involved in laser microdissection (notably M. Maître and H. Doat); and Y. Rufin at the Biochemistry and Biophysics Facility of Bordeaux Neurocampus. Confocal imaging and FRAP experiments were done at the Bordeaux Imaging Center, a service unit of CNRS-INSERM-Bordeaux University, member of the national infrastructure France BioImaging (ANR-10-INBS-04), with the help of F. Cordelières and M. Mondin. All these facilities are funded by the LabEx BRAIN (ANR-10-LABX-43). Lentiviruses were produced at the TransBioMed facility of Bordeaux University. We also thank the Electron Microscopy Research Services, Faculty of Medical Sciences, Newcastle University. This work was supported by Inserm, Agence Nationale de la Recherche (ANR) MossyPCP (ANR-12-BSV4-0016-01) (N.S., C.M., A.M.); Conseil Régional d'Aquitaine (N.S.); the Neurocampus program (M.M.); and La Fondation pour la Recherche Médicale (FRM) "Equipe FRM 2016" (DEQ20160334899) (M.M.). B.J.A.R. was an INSERM/CRA Ph.D. fellow and received funding for a fourth year from LabEx BRAIN. S.D.S.C. was supported by a European Neuroscience Campus Network (ENC-Network) Neurasmus Ph.D. fellowship and FRM 4eme annee FDT20150532542. A.Q. is funded by FRM (SPF20150934238), C.G. by the ANR PTSDMEMO, and G.B. by a return-post-doc fellowship from the Agence Nationale de la Recherche. D.J.H. was funded by British Heart Foundation grant PG/11/76/29108.

AUTHOR CONTRIBUTIONS

Conceptualization, N.S., M.M., A.D., and A.M.; Methodology, B.J.A.R., M.M.M., A.D., A.M., M.M., and N.S.; Investigation, B.J.A.R., M.M.M., S.D.S.C., C.R., M.B., A.Q., M.G., and B.A., with the help of A.S.A.A. and C.G.; Formal Analysis, B.J.A.R., M.M.M., S.D.S.C., A.D., A.M., M.B., G.B., M.M., and N.S.; Supervision, M.M.M., G.B., A.D., M.M., and N.S.; Resources, G.B. and D.J.H.; Writing – Original Draft, B.J.A.R., M.M., and N.S.; Writing – Review & Editing, N.S., M.M., A.M., A.D., S.D.S.C., M.M.M., M.G., G.B., M.B., and C.R.; Project Administration, N.S.; Funding Acquisition, N.S., M.M., A.M., and C.M.

DECLARATION OF INTERESTS

The authors declare no competing interests.

Received: September 9, 2019
Revised: March 13, 2020
Accepted: May 15, 2020
Published: June 9, 2020

REFERENCES

Altar, C.A., Jurata, L.W., Charles, V., Lemire, A., Liu, P., Bukhman, Y., Young, T.A., Bullard, J., Yokoe, H., Webster, M.J., et al. (2005). Deficient hippocampal neuron expression of proteasome, ubiquitin, and mitochondrial genes in multiple schizophrenia cohorts. Biol. Psychiatry *58*, 85–96.

Arruda-Carvalho, M., Restivo, L., Guskjolen, A., Epp, J.R., Elgersma, Y., Josselyn, S.A., and Frankland, P.W. (2014). Conditional deletion of α-CaMKII impairs integration of adult-generated granule cells into dentate gyrus circuits and hippocampus-dependent learning. J. Neurosci. *34*, 11919–11928.

Babayeva, S., Zilber, Y., and Torban, E. (2011). Planar cell polarity pathway regulates actin rearrangement, cell shape, motility, and nephrin distribution in podocytes. Am. J. Physiol. Renal Physiol. *300*, F549–F560.

Barthet, G., Jordà-Siquier, T., Rumi-Masante, J., Bernadou, F., Müller, U., and Mulle, C. (2018). Presenilin-mediated cleavage of APP regulates synaptotagmin-7 and presynaptic plasticity. Nat. Commun. *9*, 4780.

Beane, W.S., Tseng, A.S., Morokuma, J., Lemire, J.M., and Levin, M. (2012). Inhibition of planar cell polarity extends neural growth during regeneration, homeostasis, and development. Stem Cells Dev. *21*, 2085–2094.

Boutros, M., Paricio, N., Strutt, D.I., and Mlodzik, M. (1998). Dishevelled activates JNK and discriminates between JNK pathways in planar polarity and wingless signaling. Cell *94*, 109–118.

Brody, D.L., and Holtzman, D.M. (2006). Morris water maze search strategy analysis in PDAPP mice before and after experimental traumatic brain injury. Exp. Neurol. *197*, 330–340.

Casanova, E., Fehsenfeld, S., Mantamadiotis, T., Lemberger, T., Greiner, E., Stewart, A.F., and Schütz, G. (2001). A CamKIIalpha iCre BAC allows brain-specific gene inactivation. Genesis *31*, 37–42.

Clelland, C.D., Choi, M., Romberg, C., Clemenson, G.D., Jr., Fragniere, A., Tyers, P., Jessberger, S., Saksida, L.M., Barker, R.A., Gage, F.H., and Bussey, T.J. (2009). A functional role for adult hippocampal neurogenesis in spatial pattern separation. Science *325*, 210–213.

Davey, C.F., and Moens, C.B. (2017). Planar cell polarity in moving cells: think globally, act locally. Development *144*, 187–200.

Desmedt, A., Marighetto, A., Garcia, R., and Jaffard, R. (2003). The effects of ibotenic hippocampal lesions on discriminative fear conditioning to context in mice: impairment or facilitation depending on the associative value of a phasic explicit cue. Eur. J. Neurosci. *17*, 1953–1963.

Diering, G.H., and Huganir, R.L. (2018). The AMPA receptor code of synaptic plasticity. Neuron *100*, 314–329.

Dos-Santos Carvalho, S., Moreau, M.M., Hien, Y.E., Garcia, M., Aubailly, N., Henderson, D.J., Studer, V., Sans, N., Thoumine, O., and Montcouquiol, M. (2020). Vangl2 acts at the interface between actin and N-cadherin to modulate mammalian neuronal outgrowth. eLife *9*, e51822.

Du, Z., Chazalon, M., Bestaven, E., Leste-Lasserre, T., Baufreton, J., Cazalets, J.R., Cho, Y.H., and Garret, M. (2016). Early GABAergic transmission defects in the external globus pallidus and rest/activity rhythm alteration in a mouse model of Huntington's disease. Neuroscience *329*, 363–379.

Esteban, J.A., Shi, S.H., Wilson, C., Nuriya, M., Huganir, R.L., and Malinow, R. (2003). PKA phosphorylation of AMPA receptor subunits controls synaptic trafficking underlying plasticity. Nat. Neurosci. *6*, 136–143.

Feng, J., Xu, Y., Wang, M., Ruan, Y., So, K.F., Tissir, F., Goffinet, A., and Zhou, L. (2012). A role for atypical cadherin Celsr3 in hippocampal maturation and connectivity. J. Neurosci. *32*, 13729–13743.

Hagihara, H., Takao, K., Walton, N.M., Matsumoto, M., and Miyakawa, T. (2013). Immature dentate gyrus: an endophenotype of neuropsychiatric disorders. Neural Plast. *2013*, 318596.

Hagiwara, A., Yasumura, M., Hida, Y., Inoue, E., and Ohtsuka, T. (2014). The planar cell polarity protein Vangl2 bidirectionally regulates dendritic branching in cultured hippocampal neurons. Mol. Brain *7*, 79.

Heimer-McGinn, V., and Young, P. (2011). Efficient inducible Pan-neuronal cre-mediated recombination in SLICK-H transgenic mice. Genesis *49*, 942–949.

Henze, D.A., Wittner, L., and Buzsáki, G. (2002). Single granule cells reliably discharge targets in the hippocampal CA3 network in vivo. Nat. Neurosci. *5*, 790–795.

Hilal, M.L., Moreau, M.M., Racca, C., Pinheiro, V.L., Piguel, N.H., Santoni, M.J., Dos Santos Carvalho, S., Blanc, J.M., Abada, Y.K., Peyroutou, R., et al. (2017). Activity-dependent neuroplasticity induced by an enriched environment reverses cognitive deficits in Scribble deficient mouse. Cereb. Cortex *27*, 5635–5651.

Holden, H.M., and Gilbert, P.E. (2012). Less efficient pattern separation may contribute to age-related spatial memory deficits. Front. Aging Neurosci. *4*, 9.

Jawaid, S., Kidd, G.J., Wang, J., Swetlik, C., Dutta, R., and Trapp, B.D. (2018). Alterations in CA1 hippocampal synapses in a mouse model of fragile X syndrome. Glia *66*, 789–800.

Kempermann, G., Jessberger, S., Steiner, B., and Kronenberg, G. (2004). Milestones of neuronal development in the adult hippocampus. Trends Neurosci. *27*, 447–452.

Kohn, A.D., and Moon, R.T. (2005). Wnt and calcium signaling: beta-catenin-independent pathways. Cell Calcium *38*, 439–446.

Lanore, F., Labrousse, V.F., Szabo, Z., Normand, E., Blanchet, C., and Mulle, C. (2012). Deficits in morphofunctional maturation of hippocampal mossy fiber synapses in a mouse model of intellectual disability. J. Neurosci. *32*, 17882–17893.

Lee, R.C., Clandinin, T.R., Lee, C.H., Chen, P.L., Meinertzhagen, I.A., and Zipursky, S.L. (2003). The protocadherin Flamingo is required for axon target selection in the Drosophila visual system. Nat. Neurosci. *6*, 557–563.

Leutgeb, J.K., Leutgeb, S., Moser, M.B., and Moser, E.I. (2007). Pattern separation in the dentate gyrus and CA3 of the hippocampus. Science *315*, 961–966.

Marr, D. (1971). Simple memory: a theory for archicortex. Philos. Trans. R. Soc. Lond. B Biol. Sci. *262*, 23–81.

Mauriac, S.A., Hien, Y.E., Bird, J.E., Carvalho, S.D., Peyroutou, R., Lee, S.C., Moreau, M.M., Blanc, J.M., Geyser, A., Medina, C., et al. (2017). Defective Gpsm2/Gα_{i3} signalling disrupts stereocilia development and growth cone actin dynamics in Chudley-McCullough syndrome. Nat. Commun. *8*, 14907.

McHugh, T.J., Jones, M.W., Quinn, J.J., Balthasar, N., Coppari, R., Elmquist, J.K., Lowell, B.B., Fanselow, M.S., Wilson, M.A., and Tonegawa, S. (2007). Dentate gyrus NMDA receptors mediate rapid pattern separation in the hippocampal network. Science *317*, 94–99.

McNaughton, N., and Morris, R.G. (1987). Chlordiazepoxide, an anxiolytic benzodiazepine, impairs place navigation in rats. Behav. Brain Res. *24*, 39–46.

Mishra, R.K., Kim, S., Guzman, S.J., and Jonas, P. (2016). Symmetric spike timing-dependent plasticity at CA3-CA3 synapses optimizes storage and recall in autoassociative networks. Nat. Commun. *7*, 11552.

Montcouquiol, M., Crenshaw, E.B., 3rd, and Kelley, M.W. (2006a). Noncanonical Wnt signaling and neural polarity. Annu. Rev. Neurosci. *29*, 363–386.

Montcouquiol, M., and Kelley, M.W. (2020). Development and Patterning of the Cochlea: From Convergent Extension to Planar Polarity. Cold Spring Harb. Perspect. Med. *10*, a033266. https://doi.org/10.1101/cshperspect.a033266.

Montcouquiol, M., Rachel, R.A., Lanford, P.J., Copeland, N.G., Jenkins, N.A., and Kelley, M.W. (2003). Identification of Vangl2 and Scrb1 as planar polarity genes in mammals. Nature *423*, 173–177.

Montcouquiol, M., Sans, N., Huss, D., Kach, J., Dickman, J.D., Forge, A., Rachel, R.A., Copeland, N.G., Jenkins, N.A., Bogani, D., et al. (2006b). Asymmetric localization of Vangl2 and Fz3 indicate novel mechanisms for planar cell polarity in mammals. J. Neurosci. *26*, 5265–5275.

Moreau, M.M., Piguel, N., Papouin, T., Koehl, M., Durand, C.M., Rubio, M.E., Loll, F., Richard, E.M., Mazzocco, C., Racca, C., et al. (2010). The planar polarity protein Scribble1 is essential for neuronal plasticity and brain function. J. Neurosci. *30*, 9738–9752.

Nagaoka, T., Ohashi, R., Inutsuka, A., Sakai, S., Fujisawa, N., Yokoyama, M., Huang, Y.H., Igarashi, M., and Kishi, M. (2014). The Wnt/planar cell polarity pathway component Vangl2 induces synapse formation through direct control of N-cadherin. Cell Rep. *6*, 916–927.

Nakashiba, T., Cushman, J.D., Pelkey, K.A., Renaudineau, S., Buhl, D.L., McHugh, T.J., Rodriguez Barrera, V., Chittajallu, R., Iwamoto, K.S., McBain, C.J., et al. (2012). Young dentate granule cells mediate pattern separation, whereas old granule cells facilitate pattern completion. Cell *149*, 188–201.

Nakazawa, K., Quirk, M.C., Chitwood, R.A., Watanabe, M., Yeckel, M.F., Sun, L.D., Kato, A., Carr, C.A., Johnston, D., Wilson, M.A., and Tonegawa, S. (2002). Requirement for hippocampal CA3 NMDA receptors in associative memory recall. Science *297*, 211–218.

Newman, E.L., and Hasselmo, M.E. (2014). CA3 sees the big picture while dentate gyrus splits hairs. Neuron *81*, 226–228.

Ohira, K., Kobayashi, K., Toyama, K., Nakamura, H.K., Shoji, H., Takao, K., Takeuchi, R., Yamaguchi, S., Kataoka, M., Otsuka, S., et al. (2013).

Synaptosomal-associated protein 25 mutation induces immaturity of the dentate granule cells of adult mice. Mol. Brain *6*, 12.

Okerlund, N.D., Stanley, R.E., and Cheyette, B.N.R. (2016). The planar cell polarity transmembrane protein Vangl2 promotes dendrite, spine and glutamatergic synapse formation in the mammalian forebrain. Mol. Neuropsychiatry *2*, 107–114.

Paolicelli, R.C., Bolasco, G., Pagani, F., Maggi, L., Scianni, M., Panzanelli, P., Giustetto, M., Ferreira, T.A., Guiducci, E., Dumas, L., et al. (2011). Synaptic pruning by microglia is necessary for normal brain development. Science *333*, 1456–1458.

Puvirajesinghe, T.M., Bertucci, F., Jain, A., Scerbo, P., Belotti, E., Audebert, S., Sebbagh, M., Lopez, M., Brech, A., Finetti, P., et al. (2016). Identification of p62/SQSTM1 as a component of non-canonical Wnt VANGL2-JNK signalling in breast cancer. Nat. Commun. *7*, 10318.

Ramsbottom, S.A., Sharma, V., Rhee, H.J., Eley, L., Phillips, H.M., Rigby, H.F., Dean, C., Chaudhry, B., and Henderson, D.J. (2014). Vangl2-regulated polarisation of second heart field-derived cells is required for outflow tract lengthening during cardiac development. PLoS Genet. *10*, e1004871.

Rebola, N., Carta, M., and Mulle, C. (2017). Operation and plasticity of hippocampal CA3 circuits: implications for memory encoding. Nat. Rev. Neurosci. *18*, 208–220.

Rodriguez, A., Ehlenberger, D.B., Dickstein, D.L., Hof, P.R., and Wearne, S.L. (2008). Automated three-dimensional detection and shape classification of dendritic spines from fluorescence microscopy images. PLoS ONE *3*, e1997.

Rolls, E.T. (2013). The mechanisms for pattern completion and pattern separation in the hippocampus. Front. Syst. Neurosci. *7*, 74.

Ruediger, S., Spirig, D., Donato, F., and Caroni, P. (2012). Goal-oriented searching mediated by ventral hippocampus early in trial-and-error learning. Nat. Neurosci. *15*, 1563–1571.

Sabapathy, K., Jochum, W., Hochedlinger, K., Chang, L., Karin, M., and Wagner, E.F. (1999). Defective neural tube morphogenesis and altered apoptosis in the absence of both JNK1 and JNK2. Mech. Dev. *89*, 115–124.

Sahay, A., Wilson, D.A., and Hen, R. (2011). Pattern separation: a common function for new neurons in hippocampus and olfactory bulb. Neuron *70*, 582–588.

Sans, N., Ezan, J., Moreau, M.M., and Montcouquiol, M. (2016). Planar cell polarity gene mutations in autism spectrum disorder, intellectual disabilities, and related deletion/duplication syndromes. In Neuronal and Synaptic Dysfunction in Autism Spectrum Disorder and Intellectual Disability, C. Sala and C. Verpelli, eds. (Academic Press), pp. 189–219.

Schafer, S.T., Han, J., Pena, M., von Bohlen Und Halbach, O., Peters, J., and Gage, F.H. (2015). The Wnt adaptor protein ATP6AP2 regulates multiple stages of adult hippocampal neurogenesis. J. Neurosci. *35*, 4983–4998.

Schmidt-Hieber, C., and Nolan, M.F. (2017). Synaptic integrative mechanisms for spatial cognition. Nat. Neurosci. *20*, 1483–1492.

Shafer, B., Onishi, K., Lo, C., Colakoglu, G., and Zou, Y. (2011). Vangl2 promotes Wnt/planar cell polarity-like signaling by antagonizing Dvl1-mediated feedback inhibition in growth cone guidance. Dev. Cell *20*, 177–191.

Stark, S.M., Yassa, M.A., and Stark, C.E.L. (2010). Individual differences in spatial pattern separation performance associated with healthy aging in humans. Learn. Mem. *17*, 284–288.

Sun, X., Zhao, Y., and Wolf, M.E. (2005). Dopamine receptor stimulation modulates AMPA receptor synaptic insertion in prefrontal cortex neurons. J. Neurosci. *25*, 7342–7351.

Tamminga, C.A., Southcott, S., Sacco, C., Wagner, A.D., and Ghose, S. (2012). Glutamate dysfunction in hippocampus: relevance of dentate gyrus and CA3 signaling. Schizophr. Bull. *38*, 927–935.

Thakar, S., Wang, L., Yu, T., Ye, M., Onishi, K., Scott, J., Qi, J., Fernandes, C., Han, X., Yates, J.R., 3rd., et al. (2017). Evidence for opposing roles of Celsr3 and Vangl2 in glutamatergic synapse formation. Proc. Natl. Acad. Sci. U S A *114*, E610–E618.

Toni, N., and Schinder, A.F. (2015). Maturation and functional integration of new granule cells into the adult hippocampus. Cold Spring Harb. Perspect. Biol. *8*, a018903.

Torban, E., Patenaude, A.M., Leclerc, S., Rakowiecki, S., Gauthier, S., Andelfinger, G., Epstein, D.J., and Gros, P. (2008). Genetic interaction between members of the Vangl family causes neural tube defects in mice. Proc. Natl. Acad. Sci. U S A *105*, 3449–3454.

Torborg, C.L., Nakashiba, T., Tonegawa, S., and McBain, C.J. (2010). Control of CA3 output by feedforward inhibition despite developmental changes in the excitation-inhibition balance. J. Neurosci. *30*, 15628–15637.

Vivancos, V., Chen, P., Spassky, N., Qian, D., Dabdoub, A., Kelley, M., Studer, M., and Guthrie, S. (2009). Wnt activity guides facial branchiomotor neuron migration, and involves the PCP pathway and JNK and ROCK kinases. Neural Dev. *4*, 7–7.

Walton, N.M., Zhou, Y., Kogan, J.H., Shin, R., Webster, M., Gross, A.K., Heusner, C.L., Chen, Q., Miyake, S., Tajinda, K., et al. (2012). Detection of an immature dentate gyrus feature in human schizophrenia/bipolar patients. Transl. Psychiatry *2*, e135.

Weber, U., Paricio, N., and Mlodzik, M. (2000). Jun mediates Frizzled-induced R3/R4 cell fate distinction and planar polarity determination in the Drosophila eye. Development *127*, 3619–3629.

Wilson, I.A., Gallagher, M., Eichenbaum, H., and Tanila, H. (2006). Neurocognitive aging: prior memories hinder new hippocampal encoding. Trends Neurosci. *29*, 662–670.

Yamanaka, H., Moriguchi, T., Masuyama, N., Kusakabe, M., Hanafusa, H., Takada, R., Takada, S., and Nishida, E. (2002). JNK functions in the non-canonical Wnt pathway to regulate convergent extension movements in vertebrates. EMBO Rep. *3*, 69–75.

Yamasaki, N., Maekawa, M., Kobayashi, K., Kajii, Y., Maeda, J., Soma, M., Takao, K., Tanda, K., Ohira, K., Toyama, K., et al. (2008). Alpha-CaMKII deficiency causes immature dentate gyrus, a novel candidate endophenotype of psychiatric disorders. Mol. Brain *1*, 6.

Yassa, M.A., Mattfeld, A.T., Stark, S.M., and Stark, C.E.L. (2011). Age-related memory deficits linked to circuit-specific disruptions in the hippocampus. Proc. Natl. Acad. Sci. U S A *108*, 8873–8878.

Zeke, A., Misheva, M., Reményi, A., and Bogoyevitch, M.A. (2016). JNK signaling: regulation and functions based on complex protein-protein partnerships. Microbiol. Mol. Biol. Rev. *80*, 793–835.

Zhao, C., Teng, E.M., Summers, R.G., Jr., Ming, G.L., and Gage, F.H. (2006). Distinct morphological stages of dentate granule neuron maturation in the adult mouse hippocampus. J. Neurosci. *26*, 3–11.

STAR★METHODS

KEY RESOURCES TABLE

REAGENT or RESOURCE	SOURCE	IDENTIFIER
Antibodies		
Anti-Calretinin monoclonal antibody	SySy	Ref 214 111
Anti-Calretinin rabbit polyclonal antibody	Swant	Ref 7699/4
Anti-CamKII monoclonal antibody	Sigma	Ref C265
Anti-phospho-CamKII (Thr286) monoclonal antibody	Cell Signaling	Ref cs12716
Anti-cJun monoclonal antibody	Cell Signaling	Ref cs9165s
Anti-phospho-cJun (Ser243) polyclonal antibody	Cell Signaling	Ref cs2994s
Anti-Cre Recombinase monoclonal antibody	Merck Millipore	Ref MAB3120
Anti-Doublecortin X guinea-pig polyclonal antibody	Millipore	Ref AB2253
Living Colors® DsRed polyclonal antibody	Takara/Clontech	Ref 632496
Living Colors® DsRed monoclonal antibody	Takara/Clontech	Ref 632392
Anti-GAPDH monoclonal antibody	Merck Millipore	Ref MAB374
Anti-GFP chicken polyclonal antibody	Abcam	Ref Ab13970
Anti-GluA1 mouse monoclonal antibody	Merck Millipore	Ref MAB2263
Anti-phospho-GluA1 (Ser831) polyclonal antibody	Upstate	Ref 05-823
Anti-phospho-GluA1 (Ser845) polyclonal antibody	Abcam	Ref ab76321
Anti-JNK monoclonal antibody	Merck Millipore	Ref 07-175
Anti-phospho-JNK (Thr183/Tyr185, Thr221/Tyr223) monoclonal antibody	Cell Signaling	Ref cs9258
Anti-Ki67 rabbit polyclonal antibody	Abcam	Ref ab15580
Anti-NL2 guinea-pig polyclonal antibody	SySy	Ref 129205
Anti-PSD95 monoclonal antibody	Thermo Fisher Scientific	Ref MA1-045
Anti-Vangl2 rabbit polyclonal antibody	Montcouquiol et al., 2006a Montcouquiol et al., 2006b	Ref 456
Anti-VGAT goat polyclonal antibody	Frontier Institute	Ref Af620
Anti-Znt3 monoclonal antibody	Synaptic Systems	Ref 197 011
Goat anti-Rabbit Alexa 488	Invitrogen	Ref A11034
Goat anti-Rabbit Alexa 546	Invitrogen	Ref A11035
Goat anti-Guinea Pig Alexa 488	Invitrogen	Ref A11073
Goat anti-Rabbit Cy3	Jackson ImmunoResearch	Ref 111-165-144
Experimental Models: Organisms/Strains		
C57Bl6 Mouse	Janvier, France	N/A
Vangl2flox mice	Prof. D. Henderson, UK	Ramsbottom et al., 2014 Plos Genetics
CamKIIa cre mice	Prof. Dr G. Schütz (DKFZ, Germany	Casanova et al., 2001
B6.Cg-Gt(ROSA)26Sortm6(CAG-ZsGreen1)Hze/J (thereafter called Ai6 mice)	Jackson Laboratories	Stock No: 007906
Recombinant DNA		
Lenti-FUMPY	Lanore et al., 2012,	N/A
pLENTI-LV-C1ql2-ChIEFtomato-2A	Barthet et al., 2018	N/A

(*Continued on next page*)

Continued

REAGENT or RESOURCE	SOURCE	IDENTIFIER
pLENTI-LV-C1ql2-ChIEFtomato-2A-Cre	Barthet et al., 2018	N/A
AAV2/9-CaMKII(0.4)-mCherry-	Vector Bioloabs	Service request [6 × 1013 GC /ml]
AAV2/9-CaMKII(0.4)-mCherry-2A-mVANGL2 -WPRE	Vector Bioloabs	Service request [5.9 × 1013 GC/ml]
SOFTWARE		
Ethovision XT 13	Noldus	https://www.noldus.com/
VideoTrack / Rodent behavior tracking software	Viewpoint behavior Technology	http://www.viewpoint.fr/en/home
Image Lab software	BIO-RAD	Version 5.2.1
Zeiss ZEN	Zeiss	Version 2.3
Metamorph	Molecular Devices	Version 7.10
ImageJ		https://imagej.nih.gov/ij/
Neurolucida tracer software	MBF Bioscience	N/A
LAS X	LEICA	https://www.leica-microsystems.com
NeuronStudio	Rodriguez et al., 2008	N/A
Neuromatic	WaveMetrics	Igor Pro 6.0 environment
GraphPad Prism	GraphPad	Version 7
OTHER		
Digital Stereotaxic Frame, 18° Ear Bars	WPI	502300
Mouse/Neonatal Rat Adaptor	WPI	502063
UMP III (one) & Micro4 Controller	WPI	UMP3-1

RESOURCE AVAILABILITY

Lead Contact

Further information and requests for resources and reagents should be directed to and will be fulfilled by the Lead Contact, Nathalie Sans (nathalie.sans@inserm.fr).

Materials Availability

Mice lines, Adeno-associated virus and plasmids generated in this study are available from the Lead Contact with a completed Materials Transfer Agreement.

Data and Code Availability

The published article includes all statistical analysis and all full blots analyzed during this study. All the others originals data for figures supporting the current study are available from the Lead Contact on request. This study did not generate code.

EXPERIMENTAL MODEL AND SUBJECT DETAILS

Mice

Conditional knock-out mice generation

All procedures involving animals were done in accordance to the European Communities Council Directives (2010/63/EU) and the French National Committee (2013-118) recommendations. The French ''Ministere de l'Education Nationale, de l'Enseignement Superieur et de la Recherche'' approved all experiments under the authorization n°5012046-A; 01932.01; 01932.02 after agreement from the ethical committee of the University of Bordeaux. Male C57BL/6N mice were purchased from Janvier (France). Vangl2-flox mice, obtained from Prof. Deborah Henderson, had been crossed to C57BL/6 for at least 5 generations before being used for experiments (Ramsbottom et al., 2014). CamKII-Cre line (Casanova et al., 2001), obtained from Prof. Dr. Günther Schütz and colleagues (Max Plank, Germany), was intercrossed with the Vangl2-flox line and B6.Cg-Gt(Rosa)26Sortm6(CAG-ZsGreen1)Hze/J (Ai6) mice (Jackson Laboratory). Mice were genotyped using genomic DNA isolated from tails using primers: forward: CCGCTGGCTTTCCTGCTGCTG; reverse: TCCTCGCCATCCCACCCTCG. The PCR products of floxed ($Vangl2^{f/f}$) and recombined-floxed ($Vangl2^{\Delta f/f}$) allele of *Vangl2* are 541 bp and 193 bp long, respectively (see Figure 1; Figure S1). The presence of Cre-expressing transgene was detected by PCR amplification of a 240 bp product for CaMKII-Cre. Electrophoresis are run on a Labchip GXII machine from Perkin Elmer using a « DNA 5k/RNA » chip and a biochemical kit: the « HT DNA 5k ». The software (LabchipGX) of this system renders an electrophoregram that contains several peaks, which are then converted in images (Figure S1C). Beta-actin

was used as a positive control for PCR amplification. Mice were maintained under standard conditions (food and water *ad libitum*; 23 ± 1°C, 7 h–12 h light–dark cycle, light on at 7:00; experiments were performed between 9:00 and 17:00). Only male mice between 8 and 18-week-old except specified otherwise for stereotaxic injection, as stated in method details, were used and they were housed collectively in groups of five to eight in polypropylene cages for biochemical experiments and in individual cages for behavioral experiments.

Plasmids, virus and stereotaxic injection

We used a lentiviral bicistronic construct developed recently to control the expression of both the red fluorescent protein Tomato fused to ChIEF (Ch) with and without the Cre recombinase under the control of a C1ql2 minimal promoter (LV-C1ql2-Ch-Tomato and LV-C1ql2-Ch-Tomato-2A-Cre respectively) (Barthet et al., 2018). The lentiviruses were produced by the TransBioMed viral vectors facility of Bordeaux. We also used an Adeno-associated virus (AAV2/9-CaMKII(0.4)-mCherry-2A-mVANGL2-WPRE) construct purchased from Vector Biolabs (Malvern, PA 19355) to re-express *Vangl2* in the DG GCs with an mCherry fluorescent reporter. Vangl2 and mCherry transgenes were driven by a CaMKII (0.4 Kb) promoter, restricting the expression in the excitatory post-mitotic neurons, with a T2A peptide linker in between for self-cleavage co-expression. The virus titer was 5.9×10^{13} GC/ml in distilled PBS (dPBS) with 5% glycerol and was used at 1:30 in dPBS. As a control, we used a AAV2/9-CaMKII(0.4)-mCherry-WPRE with an original titer of 6.0×10^{13} GC/ml in dPBS with 5% glycerol diluted at 1:30 in dPBS.

Five-week-old Vangl2-flox or CaMKII-Vangl2$^{f/f}$ mice were anesthetized with isoflurane and injected intraperitoneally with 10% Buprecare and locally with 50% Lurocaine. They received bilateral microinjections of lentivirus control or expressing the Cre recombinase or AAV2/9 expressing the mCherry control or mCherry/Vangl2, respectively (300 nL per minute) in the DG region of hippocampus (anteroposterior [Y] −2 mm from Bregma, mediolateral [X] ± 2 mm, dorsoventral [Z] −2 mm).

METHOD DETAILS

Immunohistochemistry

Vangl2, DCX, CaR, Ki67/, DsRed, cJun, p-cJun and Cre immunohistochemistry: 10-week-old mice were perfused transcardially with 0.1 M phosphate buffer, pH 7.4 (PB), followed by 4% paraformaldehyde (PFA) in PB, brains were removed and post-fixed in 4% PFA in PB for 2 hr at 4°C. Coronal vibratome sections (40 μm) were obtained and incubated with primary antibody (see list) overnight (CaR, Ki67 and Cre) or 24 hr (Vangl2 and DCX) at 4°C, followed by Alexa Fluor 488 and Cy3 secondary antibodies for 45 min at room temperature (RT). Composite photomicrographs were acquired with a Leica DM6000 microscope equipped with a X, Y- axis stage motor and a CoolSNAPHQ2 camera (PhotoMetrics) under Metamorph software. In order to image the entire hippocampal area, stacks of 11 (in the x axis) by 11 (in the y axis) images (11*11 = 121 images in total) were acquired through horizontal zigzags by using the "Scan Stage" plugin available under the "Devices" menu and the "Stage" submenu (Metamorph software). Stitching was further achieved by using the "Montage" option under the "Stack" menu (Metamorph software). Single shot images were acquired with a Zeiss AxioImager Z1 and an AxioCam MRm. For the quantification of CaR neurons in the DG subgranular layer, positive neurons were counted live on a Zeiss AxioImager Z1 and an AxioCam MRm. For the quantification of DCX neurons in the DG subgranular layer, images were taken with the same exposure time for all genotypes on a Zeiss AxioImager Z1 and an AxioCam MRm. CaR and DCX positive neurons were then counted and averaged per lamina (superior and inferior) per DG section per brain in 3 different mice for each genotype. For the analysis of fluorescence intensity of DG granule cells immuno-labeled with either cJun or p-cJun, images were taken with the same exposure time for all genotypes on a Zeiss AxioImager Z1 and an AxioCam MRm. For both genotypes, three different regions in the upper blade of the DG were selected for further analysis. Then, DAPI staining was used to delineate the cell body of granule cells (performed on MetaMorph, Molecular Devices) and the regions created were then applied on cJun and p-cJun images. Finally, the average fluorescence intensity for these markers was retrieved in the demarked cells.

For CaR/VGAT and CaR/NL2 immunohistochemistry, animals were anaesthetized with ketamine/xylazine and perfused transcardially with ice-cold modified artificial cerebrospinal fluid (ACSF), equilibrated with 95% O_2–5% CO_2, and containing: 130 mM NaCl, 3 mM KCl, 2.5 mM $CaCl_2$, 1.3 mM $MgSO_4$, 0.58 mM NaH_2PO_4, 25 mM $NaHCO_3$ and 10 mM glucose. The brain were removed and a 5 mm thick-slice containing the hippocampus was dissected out, post-fixed in 4% PFA in PB for 1 hr at 4°C, and then cryoprotected overnight in 20% sucrose in PB before being cut into 50 μm thick coronal sections using a Leica cryostat (Du et al., 2016). Coronal sections were first incubated for 1 hr in blocking solution containing 4% donkey serum and 0.3% Triton X-100 in PB. They were then incubated for 72 hr at 4°C with primary antibodies (see list) diluted with the blocking solution, followed by 1 hr in blocking solution containing a cocktail of Alexa Fluor 488 or 647 and Cy3 conjugated secondary antibodies. Images were acquired with a BX51 Olympus Fluoview 500 confocal microscope using an oil-immersion 60x objective, 1.4 NA. CaR labeling was used to draw the outline of identified cells and define regions of interest. Quantification of the number of pre- and postsynaptic puncta on the cell periphery was performed using a custom-made macro in ImageJ software. Counts were carried out on sections obtained from four mice for each genotype.

Tissue extracts, SDS-PAGE, WB analysis

For each set of experiments, three or more hippocampi from 10-week-old mice of each genotype were processed as described previously (Moreau et al., 2010). Protein concentrations were measured using a BCA assay (Pierce, Rockford, IL) or a Bio-Rad protein

assay (Bio-Rad, Hercules, CA), and equal amount of proteins were separated with SDS-PAGE (8% or 4%–20% gradient gels) and transferred to Immobilon-P membranes. After chemiluminescence detection, films were scanned using a Molecular Dynamics (Sunnyvale, CA) densitometer. The quantifications were performed as described previously (Moreau et al., 2010). For the sake of illustration, the immunoblot images were inverted (contrast) and full blots are provided (Data S1).

Golgi impregnation method

10-week-old adult animals were perfused transcardially with 2% PFA and 2.5% glutaraldehyde in 0.1 M PB, pH 7.4. Vibratome brain sections of 100 μm were treated for 30 min with PB containing 1% osmium tetroxide, followed by an overnight incubation in 3.5% potassium dichromate, and a 2% silver nitrate solution for 6 hr. After gradual dehydration in alcohol, sections were infiltrated with Entellan® and mounted. For morphological analysis, at least 10–20 DG granule cells of the dorsal hippocampus were analyzed for each animal using camera lucida at a magnification of 100x (DMLS Microscope, Leica). Neurolucida tracer software was used (MBF Bioscience). For each neuron, all branches of basal and apical dendritic trees were reconstructed. Dendritic length was measured by Sholl analysis with respect to growing distance from the cell body. Dendritic complexity was quantified by counting the number of intersections between virtual concentric rings of 10 μm and dendritic branches. For analysis of spine density and morphology, 10 μm dendritic segments were identified, and number of spines present and their head size were measured as described previously (Moreau et al., 2010).

Timm's staining

The FD Rapid TimmStain Kit (FD NeuroTechnologies, Inc.) was used. Ten-week-old adult animals were perfused transcardially for 10 minutes with the perfusate A and B freshly made, immediately followed by 4% PFA in 0.1 M PB, pH 7.4 for 10 minutes (around 100 mL for each solution). After 24 hr postfixation in 4% PFA in PB at 4°C, 50 μm vibratome sections of the brain were cut, mounted on gelatin coated slides and dried for 48 hr at RT. Sections were incubated in the staining solution (made freshly by mixing TimmStain Kit's solutions A, B, C and D) for 50 minutes at 30°C in the dark with a gentle shaking. After gently washing under running water for 30 minutes, sections were gradually dehydrated in alcohol, cleared in xylene, and mounted with Entellan.

Quantification of dendritic spines

Eight- to nine-week old CaMKII-Cre/Vangl2$^{f/f}$ mice received unilateral stereotaxic microinjections of a lentivirus (1000 nL at 300 nL per min) expressing YFP under the control of the promoter HubC (FUGW_MyrPalmYFP_FUMPY, titer 2.18x107 GC/ml) in the DG region of hippocampus (anteroposterior [Y] −2 mm from Bregma, mediolateral [X] ± 2 mm, dorsoventral [Z] −2 mm). Ten days after surgery, the animals were perfused transcardially with PB followed by 4% PFA in PB, the brains were removed and post-fixed in 4% PFA in PB for 24 hr at 4°C. Free-floating vibratome coronal sections (50μm) were incubated with anti-GFP and anti-CaR (rabbit) primary antibodies at 4°C overnight, followed by Alexa Fluor 488 and Cy3 conjugated secondary antibodies for 1 hr at RT. Stacks of images were acquired with a confocal microscope (Leica SPE, oil objective 63X, 1.4 NA, zoom 2.5) and the molecular layer (ML) of the DG was divided into 3 layers: Inner (IML, visualized with CaR-positive labeling), Middle (MML) and Outer (OML). The number and type of spines were counted and classified, respectively, with the software NeuronStudio (Rodriguez et al., 2008). For each animal, 20 samples of 10-μm length of dendrites were analyzed per layer. Normality of distribution was assessed with a D'Agostino & Pearson normality test. When normal, the data were analyzed with an unpaired t test, otherwise they were analyzed with a Mann-Whitney test.

Neuronal cell culture

Coverslip coating

Regular 18-mm glass coverslips were incubated for 2 h at 37°C with 30 μg/ml poly-L-lysine (PLL) in borate buffer (at pH: 8.5), rinsed with H_2O, then incubated ON at 4°C with an acid boric (at pH: 8.4) solution containing 2μg/ml laminin (Ref L2020, Sigma-Aldrich). Finally, for coverslips were rinsed and incubated with Neurobasal 2h at 37°C before neuron plating.

Culture

For hippocampal neurons culture, hippocampi were harvested from E18 rat pups in a HBSS solution, enzymatically and mechanically dissociated (Mauriac et al., 2017). After 14 min incubation at 37°C in trypsin, the hippocampi were rinsed with a Plating Medium (PM) that contains neurobasal medium, B27 supplement (50X, GIBCO), 2 mM Glutamine, 0.3% Glucose, 37.5 mM NaCl and 5% of Fetal Bovine Serum (FBS). The hippocampi were dissociated by gentle up and down movements though a Pasteur pipette, and then centrifuged at 1 rpm, 5 min at room temperature (RT) after counting. The neurons were further diluted in 1 mL of PM and plated on the previously prepared coverslips. Two hours after plating, the PM was replaced by a similar medium without serum.

FRAP and analysis

Fluorescence-recovery-after-photobleaching (FRAP) experiments were performed on a Leica DMI8 (Leica Microsystems, Wetzlar, Germany) equipped with an HCX PL Apo CS2 63x oil NA 1.4 objective and a camera sCMOS Prime 95B camera (Photometrics, Tucson, USA). Photo-manipulation experiments were done with a iLas^2 scanner system (Gataca Systems, Massy, France) using the same Laser bench as for imaging. The 37°C atmosphere was created with an incubator box and an air heating system (PeCon GmbH, Germany). This system was controlled by MetaMorph software. After acquiring a 2 s baseline at a frame rate of 5 Hz, rapid photobleaching of 5 to 10 spines expressing GluA1-SEP (and DsRed or DsRed-Vangl2) was achieved at higher laser power (10

repetition cycles). Fluorescence recovery was further recorded for 210 s at a frame rate of 0.3-1 Hz. For FRAP analysis, a macro designed by Fabrice Cordelieres was used (Bordeaux Imaging Center, BIC, Bordeaux, France). Briefly, fluorescence values (*Ft*) were corrected 1) for the background noise by subtracting the average fluorescence intensity of the background (BG) to the fluorescence detected in the photobleached regions (SEP) as well as in a control region (*Ct*) that has not been photobleached; and 2) for incidental photobleaching by dividing those values by the average fluorescence detected in the control region (*Ctc, Ct corrected*). Fluorescence values detected in the photobleached areas are then normalized (*Ft Norm*) for each time point (*Ft*), by dividing these values by the average fluorescence intensity (also corrected) detected during the prebleach acquisition (*F*0).

$$FT = \frac{SEP - BG}{Ctc}$$

$$Ft\ Norm = \frac{Ft}{F0}$$

Electron Microscopy Analysis

All procedures were performed according to the requirements of the United Kingdom Animals (Scientific Procedures) Act 1986 and Newcastle University AWERB 374. 12-week-old male mice (3 per genotype) were terminally anesthetized by a brief inhalation of isoflurane (0.05% in air) and intraperitoneal injection of ketamine (100 mg/kg) and xylazine (10 mg/kg), and then transcardially perfused with 2% PFA and 2.5% glutaraldehyde in 0.15 M cacodylate buffer (pH7.4) with 2mM calcium chloride. The brains were dissected and stored in the same fixative at 4°C, overnight. Vibratome sections (200 μm) were cut, collected in 0.1M phosphate-buffered saline (PBS; pH 7.2), postfixed in 1.5% (w/v) potassium ferrocyanide in 2% (v/v) osmium tetroxide in PBS (1 hr, 4°C), followed by: 1% (w/v) thiocarbohydrazide in ddH_2O (20 minutes, 60°C), 2% (v/v) osmium tetroxide in ddH_20 (30 minutes, RT), 1% (w/v) uranyl acetate (aqueous) (overnight, 4°C), Walton's lead aspartate solution (30 minutes at 60°C). Note each step was followed by ddH_2O rinses. The sections were then dehydrated in an ascending scale of ethanol, infiltrated and flat embedded in Durcupan epoxy resin. The DG region of the hippocampus was trimmed and embedded in resin blocks for further semithin and ultrathin sectioning with a Leica UC7 ultramicrotome and visualized with a Philips CM100 transmission electron microscope (FEI) at 100 kV. The images were captured with an AMT XR40 4 megapixel side mounted CDD camera at a magnification between 7900 and 92000. Only identified synapses on dendritic spines of apical dendrites of GC in DG OML were included in the analysis. No tangentially cut synapses were analyzed. To determine the spine density (number of spine/μm^2), we utilized 10–15 images per animal (7900 magnification, single image area = 176.95 μm^2) in which we identified the spines and, then, quantified them using the cell counter tool in ImageJ (https://imagej.nih.gov/ij). The average thickness of the postsynaptic density (PSD) was measured as described previously (Moreau et al., 2010). The measurements and analyses were all performed by experimenters blind to the genotype.

EM Statistical analysis

For the quantitative analysis of electron microscopy data, statistical analyses were performed using Sigmaplot11 (Systat Software). When data populations had a Gaussian distribution according to the Shapiro-Wilk test, we reported parametric statistical features; otherwise we performed the nonparametric statistical Mann–Whitney rank sum test followed by Kolmogorov–Smirnov test to assess statistical significance between groups. All data are presented as mean ± SEM; $p < 0.05$ was considered statistically significant.

Electrophysiological recordings

Slice preparation

Parasagittal hippocampal slices (300-330 μm thick) were obtained in 10 to 13-week-old mice. Animals were anesthetized with intraperitoneal ketamine/xylazine injection (75 and 10 mg/kg, respectively) or 4% isoflurane. After checking their reflexes, decapitation was performed. The brain was quickly removed and immersed in ice-cold cutting solution (the composition is given below). The hemispheres were separated by a sagittal cut in the corpus callosum and each one was glued and mounted onto a Leica VT 1200S vibratome. Brain slices were made with by a razor blade with an angle of ~17° at 0.05 mm/s. All the preparation was performed under oxygenation (95% 0_2 and 5% CO_2), in an ice-cold cutting solution (in mM): 87 NaCl, 25 $NaHCO_3$, 10 glucose, 75 sucrose, 2.5 KCl, 1.25 NaH_2PO_4, 0.5 $CaCl_2$, and 7 $MgCl_2$. Right after slicing, slices were then transferred into a holding chamber at 35°C during 30 minutes for recovery and were then placed at RT for the duration of the experiment. Slices were transferred to a recording chamber in which they were continuously superfused with an oxygenated extracellular medium (95% O_2 and 5% CO_2) containing (in mM): 125 NaCl, 2.5 KCl, 2.3 $CaCl_2$, 1.3 $MgCl_2$, 1.25 NaH_2PO_4, 26 $NaHCO_3$, 10 glucose, pH 7.4. A Bicuculline (10 μM)/CGP 55845 (3 μM) mix or a Picrotoxin (50 μM)/CGP54626 (3μM) mix were present in all experiments in order to block $GABA_A$ and $GABA_B$ receptors, respectively.

Electrophysiological recordings

Recordings were performed at 30°C in voltage-clamp clamp mode from DG GCs using borosilicate pipettes (Harvard apparatus: 1.5 OD x 0.86 ID) pulled with a micropipette puller (P97, Sutter Instruments, Novato, CA), which had resistances between 3 and 4.5 MΩ. The patch electrodes were filled with a solution containing (in mM): 140 $CsCH_3SO_3$, 2 $MgCl_2$, 4 NaCl, 5 phospho-creatine, 2 Na_2ATP, 0.2 EGTA, 10 HEPES, 0.33 GTP, pH 7.3 adjusted with CsOH.

To analyze basal synaptic transmission and plasticity evoked EPSCs were recorded in DG GCs in the whole-cell patch clamp mode by stimulating the lateral performant path (LPP) with a glass microelectrode placed in the outer molecular layer (OML). mEPSCs were recorded in the presence of TTX (0.5 mM) and D-APV (50 mM) while holding the cells at −70 mV. The AMPAR/NMDAR ratio was calculated as the peak averaged AMPAR EPSC (15 consecutive events) at −70 mV divided by the averaged NMDAR EPSCs (15 consecutive events) measured at 40 ms after the onset of the dual component EPSC at +40 mV.

For LTP experiments in the DG, evoked field excitatory post-synaptic potentials (fEPSPs) were recorded in the outer molecular layer of the DG using a glass pipette (1-3 MΩ) filled with extracellular medium. The glass stimulating electrode was placed in the outer molecular layer at 200 μm away from the recording pipette. The stimulation intensity was set to produce 40%–50% of maximum response. LTP was induced by applying a high frequency stimulation (HFS) protocol consisting of 100 Hz trains of stimuli for 1 s repeated 3 times at 10 s intervals. To generate summary graphs, individual experiments were normalized to the baseline and were averaged to generate 1-minute bins. These were then averaged together to generate the final summary graphs. The magnitude of LTP was calculated based on the fEPSP values 50-60 minutes after the end of the induction protocols. All drugs were obtained from Tocris Cookson (Bristol, UK) or Hellobio (Bristol, UK).

Data acquisition and analysis

Recordings were made via Patchmaster 2.71 using an EPC10 amplifier (HEKA Elektronik, Lambrecht/ Pfalz, Germany), filtered at 0.5–1 kHz, digitized at 5-10 kHz, and stored on a personal computer. Analysis was performed using Neuromatic (www.neuromatic.thinkrandom.com) written within the Igor Pro 6.0 environment (WaveMetrics, Lake Oswego, OR). Values are presented as mean ± SEM. Either paired or unpaired non-parametric tests were used to assess statistical differences between values using Prism 7. No statistical methods were used to predetermine sample sizes, but our sample sizes are similar to those generally employed in the field. No data point (outlier) was removed from the collected datasets. N mentioned in the paper represents a single measurement from a single cell. We considered biological replication each different cell. During both the experiments and the analysis, the experimenter was blind to the genotype of the animal used.

Behavioral testing

Behavioral experiments were conducted during the light phase of a 12 hr light/dark cycle, under conditions of dim light and low noise. All animals had been weighed twice a week from 8 to 18 weeks of age. Mice were tested in activity cages for their locomotor activity, in open field test for their exploratory activity and anxiety-like behavior, and in Morris water maze for their spatial learning and memory performances.

Y-Maze

The Y-maze was used as a behavioral test that assessed the exploration of mice in a new environment and the short term memory, based on measuring the spontaneous alternation. The apparatus is a Y shaped maze with 3 white plastic arms with a length of 30 cm, width of 8 cm, and wall height of 12 cm. The mice are placed in the middle of the maze and allowed to freely explore each arm during 5 min. After the test, the mice are returned to their homecage. The percentage of alternation and the distance moved in each arm are measured using videotracking (Ethovision).

Plus-Maze

The elevated plus maze test allows a measure of anxiety-related behavior. The apparatus is a cross shaped maze with two open (30 × 5 cm) and two closed (30 × 5 x 20 cm) opposed arms with a central platform in the center of the cross (5 × 5 cm). The walls of the closed arms are black, the floor of the maze is white and the maze is elevated 1 m above the ground. The mice are placed in the central platform and allowed to freely explore each arm during 5 minutes. After the test, the mice are returned to their homecage. The time spent and the numbers of entries in open and closed arms are measured using videotracking (Ethovision).

Open field and novel object

The open field test evaluates the global locomotor activity and the exploration of a new environment. The open field is a square shaped arena (40x40 cm) with wall height of 40 cm. The mice are placed in the center of the arena and allowed to freely explore the environment during 10 min. After the test, the mice are returned to their homecage during 30 min. An object is set in the center of the arena and the mice are put back in the open field during 10 min, with the object. The mice are finally returned to their homecage. The percentage of time spent and distance moved in the center of the arena are measured to assess the exploration of the new object in the known arena using videotracking (Ethovision).

Light/dark box

The Light/dark box tests the anxiety-related behavior using the innate willingness of exploration and aversion of brightness in mice. The apparatus is a box (40x20 cm) divided in two, a bright and a dark compartment separated by a wall with a hole that allows the mice to move freely from one compartment to the other. The mice are placed in the bright box and allowed to freely explore each compartment during 5 minutes. After the test, the mice are returned to their homecage. The time spent and distance moved in bright and dark boxes are measured using videotracking (Ethovision).

Morris water maze / Pattern completion

In this experiment, the water maze evaluates the ability of mice to orient them in space, using spatial cues to find a platform that allows them to escape the water. When mice have learned the spatial map to find this platform, some cues are removed. The mice have to find the platform with the remaining cues. We test here the ability of rebuilding the spatial map named "pattern completion." The apparatus is a circular arena (ø 150 cm) filled with water (19-20°C) mixed with white nontoxic dye. A video camera fixed to the ceiling of the room was

used to collect and transmit data to a computerized tracking system (Viewpoint) located in an adjacent room. The experiment has three phases, visual learning, spatial learning, and probe tests. Visual learning: first, the mice are tested in their ability to swim, their willingness to escape the water, and their visual acuity. The platform is cued and the mice are allowed to freely swim in the water during 1 minute. If the mice find the platform, they are returned to their homecage. Otherwise they are guided to the escape platform. The latency to reach the platform is measured to assess the visual learning. Spatial learning: next, when the mice have learned how to find the platform, the cue is removed to allow the spatial learning. The mice have to use the external spatial cues placed around the water maze to localize the platform. They are put in the water with a different starting point and they are allowed to swim freely during 1 minute. The latency to reach the platform is measured to assess the spatial learning. Strategies to locate the platform were quantified manually and blindly regarding the genotype and classified according to previous criteria (Brody and Holtzman, 2006). Probe tests: three probe tests are used to confirm the spatial learning and the "pattern completion" during which the platform is removed. The mice are placed in the water maze and allowed to swim freely during 1 minute. The latency to reach the phantom platform (PPF, means the platform location), the time spent, and the distance moved in this PPF are measured. First, the "all cues" probe test evaluates the spatial learning. Next, the "partial cues" probe test, in which most of the cues are removed, assesses the "pattern completion." Finally, the "no cue" probe test, in which all the cues are removed, allows to show the specificity of the previous spatial learning and "pattern completion" probe tests. Between each probe test, mice have a spatial training to avoid extinction.

Radial maze / Pattern separation

In this experiment, the radial maze allows us to evaluate the ability of the mice to discriminate similar information before their storage, named "pattern separation." The apparatus is an elevated 8-arm maze with a central platform fully automatized by videotracking (IMETRONIC Pessac- France). At each end of arm, there is a dispenser of food pellets. The opening and closure of each arm is automatic. The test uses the ability of mice to choose the non-visited arm to get the pellet. After having visited an arm, the mice have to choose between two arms, the previous one, already visited with no more food, and the new one with a food pellet. The mice have to learn this rule to get the food: if they choose the new one, it is a correct answer, otherwise it is a wrong one. To assess the use of the "pattern separation," the angle between the two arms is different for each trial. Smaller is the separation, higher is the difficulty of the test and higher is the demand in "pattern separation." The mice are placed in the center platform and can freely explore the opened arm to get the food. When the mice are back in the middle, the arm is closed. Then the previous arm and a new one (with the food) are opened. The mice have to choose one arm to get the food. Next the mice go back in the middle, the arms are closed and a new session begins, with new random arms. The training lasts 8 days during which corrects answers are measured.

Fear conditioning / Pattern separation

Every day for 8 days, the mice are exposed to two similar contexts, in the morning and in the afternoon in a pseudo-random manner. These two contexts are similar in volume (10 m^3) and brightness (80 lux) but differ by the experimental materials they contain and by the cues placed on their walls. Thus, these two contexts only differ in their background distal cues, the proximal cues provided by the conditioning chamber remain the same across testing. Moreover, in order to limit the possibility of a simple direct association between the shock and one particular static contextual feature, an effort was made to prevent any of the distal cues to be more salient than the other ones (Desmedt et al., 2003).

In the conditioning context (C), mice are placed in a chamber for 2 minutes, then exposed to a 2 minutes tone (1000 Hz – 63 dB) spaced of 30 s from a mild foot-shock (0.4 mA – 1 s) (trace conditioning). The tone, being the most salient (phasic) cue present in both contexts is used in order to contrast with all the other (tonic) contextual cues, preventing thereby a "contextual" discrimination based on an elemental strategy: its saliency limits any potential simple association between a simple tonic contextual cue and the unconditional stimulus (US). In the neutral context (N), mice never receive any foot-shock. We quantified the freezing behavioral response (blind analysis) defined as a complete immobility lasting more than one second (except for respiratory movements). In order to quantify the contextual discrimination, we measured the freezing time during the first 2 minutes exposure to each context, using the tone period as an internal control (data not shown). The level of freezing in each context is measured to evaluate the contextual fear conditioning and the comparison between the freezing in the neutral and the conditioning context allows us to assess the "pattern separation."

QUANTIFICATION AND STATISTICAL ANALYSIS

No method of randomization to assign experimental groups was performed but they are similar to those reported in previous publications (Hilal et al., 2017; Moreau et al., 2010). Data collection and analysis were performed blind to the conditions of the experiment. All animals were assigned randomly to the different experimental conditions. Normality and homogeneity of variances from the samples were tested with Shapiro-Wilk test and Bartlett test respectively. If data were parametric, Student's t test (two comparisons), ANOVA 1-way (multiple comparisons), ANOVA 2-way or ANOVA 3-way were used. Otherwise non-parametric tests were used (Mann-Whitney or Kruskall-Wallis). When significant interaction effects of main factors were detected, post hoc analyses, recommended by GraphPad Prism 7 software (Bonferroni's, Sidak's or Tukey's for ANOVA and Dunn's for Kruskall-Wallis), were performed. Effects with p values ≤ 0.05 are reported as significant. The exact value of n, what they represent as well as SEM or SD graphic display are indicated in figure legends. Detailed information about statistical tests used and their results are provided in an excel statistical Table (Table S1).